

Novel Nuclear Fusion-Enhanced Water-Fueled Propulsion Offers Outstanding Potential for Future Space Exploration

Wesley Faler
Miles Space, Inc.
Tampa, FL, USA
wes@miles-space.com

Brad Berkson
Miles Space, Inc.
Tampa, FL USA
brad@miles-space.com

This paper presents a novel electric propulsion system that uses pulsed plasma and ion-electron recombination to generate thrust primarily from internal pressure, using water vapor as propellant. In-space testing of the Poseidon™ thruster demonstrated 37.49 mN average thrust and over 4,800 seconds specific impulse at under 1.5 W input power. A physics-based model captures the full mass, energy, and momentum balances and matches experimental results, supporting pressure as the dominant thrust mechanism. Experimental detection of proton–boron fusion in the exhaust plume further validates the system's plasma behavior and confirms a key element of its operating cycle.

Keywords: electric propulsion, pressure thrust, pulsed plasma, water propellant, ion-electron recombination, proton–boron fusion, in-space testing



Table of Contents

1. Introduction.....	3
2. Poseidon™ Thruster Operating Principles.....	4
2.1 Overview	4
2.2 Foundations of Pressure-Based Thrust.....	6
3. Equation Model – Mass, Energy, Momentum Balances.....	7
3.1 Model and Equations	7
Overview	7
Details.....	8
Equations	11
Efficiencies.....	17
3.2 Equation Solving.....	18
4. In-Space Test Results 2024-09.....	20
4.1 Poseidon™ Thruster Model M1.5	20
4.2 Setup and Results Summary	21
5. Ground Test Results at Miles Space	22
5.1 Setup and Results Summary	22
5.2 Typical Calibration #202405080900	24
5.3 Typical Experiment #T202405081004	24
5.4 Typical Experiment #T202405151412.....	26
6. Model Results.....	27
6.1 Model Results for In-Space Test.....	27
6.2 Model Results Comparisons.....	31
7. Water Propellant and Plasma Properties	33
8. Proton-Boron Fusion	34
8.1 Background	34
8.2 Simulation of Proton-Boron Fusion	37
8.3 Physical Experiments	45
8.4 Fusion Discussion.....	50
9. Conclusions	50
10. References and Additional Reading.....	51



1. Introduction

Electric propulsion has long been defined by the efficient acceleration of charged particles, with thrust derived almost exclusively from momentum exchange. The Poseidon™ thruster introduces a new paradigm: an electric propulsion system in which thrust arises primarily from pressure forces generated within a pulsed plasma cycle. This effect, long predicted by canonical propulsion theory but largely neglected in electric propulsion design, is shown here to be not only real but dominant.

The Poseidon™ architecture utilizes pulsed electrostatic acceleration, virtual cathode formation, and pressure management via ion-electron recombination to produce thrust using water vapor as propellant. In-space testing has demonstrated average thrust exceeding 37 mN at under 1.5 W input power, with specific impulse over 4,800 seconds—marking a significant advancement in low-power propulsion capability.

The thrust model is rooted in first-principles conservation of mass, energy, and momentum, and accounts for the dynamic behaviors unique to pulsed plasma operation. Unlike conventional models, this framework retains the pressure term in the thrust equation, providing critical explanatory power for observed performance.

Further, the paper presents experimental evidence of proton–boron (p–B) fusion occurring in the thruster's exhaust plume, made possible by the presence of high-velocity protons and targeted boron injection. Gamma detection and alpha-particle modeling confirm this fusion behavior, which further supports the proposed operating cycle and enhances plasma dynamics through ambipolar diffusion and plume ion sheath reinforcement.

This work details both theoretical modeling and empirical results from in-space and ground-based testing. The findings support a propulsion concept that challenges established assumptions, offers substantial gains in efficiency, and opens new avenues for future missions—including those relying on in-situ water resources and low-power platforms.



2. Poseidon™ Thruster Operating Principles

2.1 Overview

The physical structure of a Poseidon™ thruster is seen in 3D in the following figure. It is a thin, planar structure.

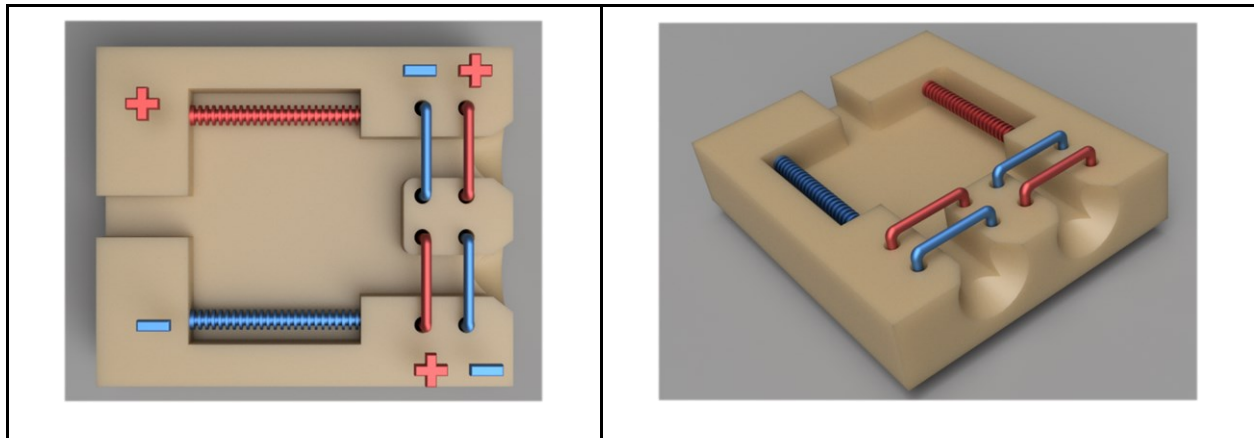


Figure 1 Physical structure of a Poseidon™ thruster. (left) Top view. (right) Iso view showing exit nozzles.

From Figure 2, a Poseidon™ thruster has:

- a planar plasma formation region containing spark electrodes
- two exhaust ports, each ringed by acceleration electrodes
- a single power supply providing spark and acceleration power

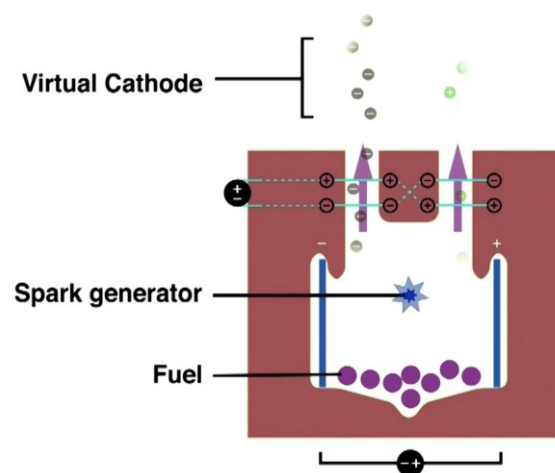


Figure 2 Poseidon™ operation schematic

Each exhaust port is ringed with high voltage electrodes. One exhaust port's voltage acts to focus and extract positive ions from the plasma. The other port affects electrons.



Operation is cyclic with several concurrent events, as outlined below.

- Vapor enters the plasma formation region, expanding and changing pressure on its path towards the exhaust ports. Paschen's law ensures a spark occurs within the vapor at the point where the supply voltage meets the pressure on the Paschen curve. The spark causes a shockwave that flows backwards to the fuel supply, stopping incoming flow briefly.
- Due to mass differences, electrons leave the plasma before ions, generating thrust from their interaction with the acceleration electrodes. Once outside the thruster, the electrons form a virtual cathode that pulls upon the ions remaining within the thruster.
- As the ions leave, thrust is obtained from acceleration electrodes. However, the ions also derive kinetic energy from the virtual cathode, slowing the exhaust electrons. This gives an increased acceleration voltage upon the ions (but not upon the force imparted to the acceleration grid).
- At this point in the cycle, the exhaust region has a distant electron cloud and a nearer ion cloud. There is a net-positive, partially ionized plasma still within the reaction chamber. Because the incoming fuel supply has been briefly stopped from the spark-induced shockwave, plasma is not being replenished.
- A potential energy peak arises from the charge arrangement. Along the axial line from fuel inlet to exhaust ports, the peak occurs midway along the axially oriented spark electrodes. Ions on the interior side are trapped by this peak, with only the hottest ions having enough energy to overcome the peak. Ions on the exhaust side are accelerated into the plume. This peak is the expression of the repulsion of interior ions with plume ions, a repulsion not overcome by the plume electrons due to their greater distance.
- The relatively cold trapped interior-most plasma undergoes some recombination. Recombination is an exothermic reaction, releasing the energy initially required for ionization. The neutral gas formed from ion-electron recombination is pressurized and heated as a result. The neutral gas, a mix of the original unionized gas and the recombined plasma, collides with the trapped ions. The trapped ions have axial momentum, being repelled by the plume ions, and transfer this momentum to the colliding neutrals. Thus, the neutrals gain axial momentum toward the interior face of the thruster where they collide with the wall and generate a pressure force.
- As the plume advances, the potential energy peak diminishes, and trapped ions exit. Likewise, increasingly cold trapped plasma undergoes more recombination. Eventually, the cycle ends with neutrals exiting as propellant inflow flow overcomes the backflow shockwave, and the cycle repeats.

In all, recombination is used to make pressurized neutrals at a beneficial location and collisions with ions are used to retain the pressurized neutrals for a useful period. Pressure-style momentum normally transferred to an interior wall is instead coupled into ions in the plume, leaving a net force against the physical structures of the thruster. Imbalance in charge carrier masses ultimately set up the electric field that fosters the cooling needed for preferential recombination to occur.

Pressure-style thrust is the primary method of thrust creation. Comparatively, only small amounts of thrust are generated by electrostatic acceleration of charged particles, by the Lorentz force



acting on the spark along the linear electrodes (as is done with pulsed plasma thrusters), or by cold gas.

2.2 Foundations of Pressure-Based Thrust

The thrust from a rocket, even an electric rocket and even in space, has two sources:

- Momentum – momentum gained by accelerating matter
- Pressure – force from an imbalance in containment of pressurized propellant

The thrust equation of a generic rocket (chemical or plasma) is taken from Newton's laws stating that the sum of forces on an object is equal to the momentum of the exiting particles. The sum of forces includes force from accelerating exiting particles as well as force due to pressure. An algebraic rearrangement then yields the rocket thrust equation:

Equation 1 Rocket thrust equation

$$F = \dot{m}v_{ex} + A_e(p_e - p_a)$$

Where:

- F is the thrust force
- \dot{m} is the mass flow rate
- v_{ex} is the exhaust velocity of the flowing matter
- p_e is the pressure within the engine at its exhaust exit plane
- p_a is the ambient pressure
- A_e is the area of the exhaust exit region

The thrust equation applies in vacuum as well as in atmosphere, to both chemical rockets and electric plasma thrusters.

The literature teaches that the pressure term is intrinsic and cannot be removed by changing the control volume over which an analysis is done as no new control volume can eliminate the need to sum all forces. With vacuum conditions at zero and design factors traditionally favoring zero exit pressure, it is convenient to drop the pressure term. An argument that the term is near zero does not eliminate its presence from the underlying physics.

The pressure term is the largest source of contention when relating thruster observations to theory. The electric propulsion industry rarely, if ever, needs the term. Indeed, unlike the chemical rocket industry, the foundational books for electric propulsion going back to the 1950's present only the momentum term for the thrust equation. The same books do mention pressure thrust in the prose, quickly dismissing it due to design preferences to drive engine exhaust pressure to zero. Indeed, most articles in both industries quickly move to the topic of nozzle design believing that the velocity gain from optimal nozzle design more than compensates for the reduction in pressure thrust.

Readers unaccustomed to considering pressure terms, especially those convinced that the pressure term is mistakenly included and does not exist in physical reality, are encouraged to reference [Ref. 20], [Ref. 21], and [Ref. 22].



The Sutton book [Ref. 20] is frequently referenced and historically regarded as authoritative. The Ulrich book [Ref. 21] has a thorough integral-based derivation and concludes that the momentum term is merely a simplification of the essential pressure term. Ulrich is also particularly rigorous with vector directions, noting the common slang where mass flow being expressed as a positive term when it is really a negative number being the derivative of rocket mass.

A mathematical convenience is to reduce the thrust equation by choosing an “*effective* exhaust velocity”. The effective exhaust velocity is not the true physical exhaust velocity, not even an RMS measurement of it, so take care not to use it when calculating kinetic energy. Especially do not use it in other non-linear equations that are susceptible to the statistical “flaw of averages” fallacy (see [Ref. 14] and [Ref. 15]) in which linear averages are applied to non-linear terms, yielding false answers compared to a correct study that embraced the distribution of input values.

Equation 2 Use of “effective exhaust velocity”

$$F = \dot{m}v_* = \dot{m}v_{ex} + A_e(p_e - p_a)$$

$$v_* = \frac{F}{\dot{m}} = v_{ex} + \frac{A_e(p_e - p_a)}{\dot{m}}$$

Where:

- v_* is the effective exhaust velocity (not physically measurable).

Specific impulse is calculated from thrust and mass flow, with the convention of using weight-specific impulse (hence the inclusion of the “g” term for Earth standard acceleration due to gravity). As a mathematical convenience, the effective velocity can be used, but not the actual exhaust velocity when pressure has contributed to the thrust.

Equation 3 Specific Impulse definition

$$I_{sp} = \frac{T}{\dot{m}g} = \frac{v_*}{g}$$

When pressure is present, power is not calculable from exhaust velocity. Rather, a model must be presented that accounts for the energetic source of the pressure, ionization energy, etc.

3. Equation Model – Mass, Energy, Momentum Balances

3.1 Model and Equations

Overview

The model is based upon the following assertions of device operation. These assertions are later detailed into variables and equations that balance mass, energy, and momentum.

Ion-electron recombination makes neutral gas. Recombination is an exothermic reaction, releasing the energy initially required for ionization. The neutral gas formed from ion-electron recombination



is pressurized as a result. Ions on the interior side of the potential well are trapped. These trapped ions have momentum in the axial direction due to their repulsion from ions in the plume. This anisotropic momentum gets transferred to pressurized neutrals, trapping them as well.

Energy is expended for ionization. Some of that energy goes toward making neutral gas through recombination. Therefore, the energy terms for ionization and flow of pressurized gas are related such that ionization energy exceeds pressurized gas flow energy.

Thrust is related to exit momentum and to pressure.

Power is related to volumetric gas flow rate as well as to kinetic energy of accelerated particles. Flowing neutral gas requires power to pressurize and undergo translation motion. The translation velocity, aka “bulk velocity”, of the neutral gas depends upon the volumetric flow rate and exit aperture area.

An ion-forming spark causes a shockwave that flows backwards to the fuel supply, stopping incoming flow briefly. Pressurization of neutrals near the inlet region further inhibits the flow of new material. Thus, mass flow into the reaction chamber becomes pulsed, occurring only during the times in which no thrust is being made. Pulsed flow occurs between the gas flow choke point and the exhaust with pressurization events in the downstream plenum not interfering with choked flow conditions.

Measured input mass flow rate is the arithmetic average of the instantaneous flow rate into the reaction chamber – a point downstream from the choked flow point. Measured input mass flow rate is also the continuous flow rate leaving the propellant tank, which being upstream from the choke point, is not affected by pulses in downstream pressure.

Specific impulse, I_{sp} , is calculated using the measured force and measured mass flow. That is, specific impulse is derived from the time average values for force and mass flow. Because the entirety of the behaviors over an operating cycle are necessary, instantaneous I_{sp} at any single moment is not relevant to mission planning.

Details

High voltage generation is done using step up transformers. Low voltage pulsed DC power is applied and pulsed high voltage DC power is created. The process is pulsed such that during low voltage power intake, no high voltage is present. The pulses are generated by an analog circuit with frequency and duty cycle set to maximize high voltage.

A second pulse pattern is overlaid upon the high voltage generation pulses. This is termed the “firing pattern”. It is a blanking pattern that determines when the high voltage pulse cycles are permitted and when they are entirely omitted, even skipping drawing of power. Together, these patterns form the operating cycle. The relationship between these patterns is shown in the figure below. Duty cycle fractions, n_{hv} and n_{fp} , are critical to the model as they, with the cycle frequency, set the duration during which thrust is made, cold gas flows, and power is consumed.

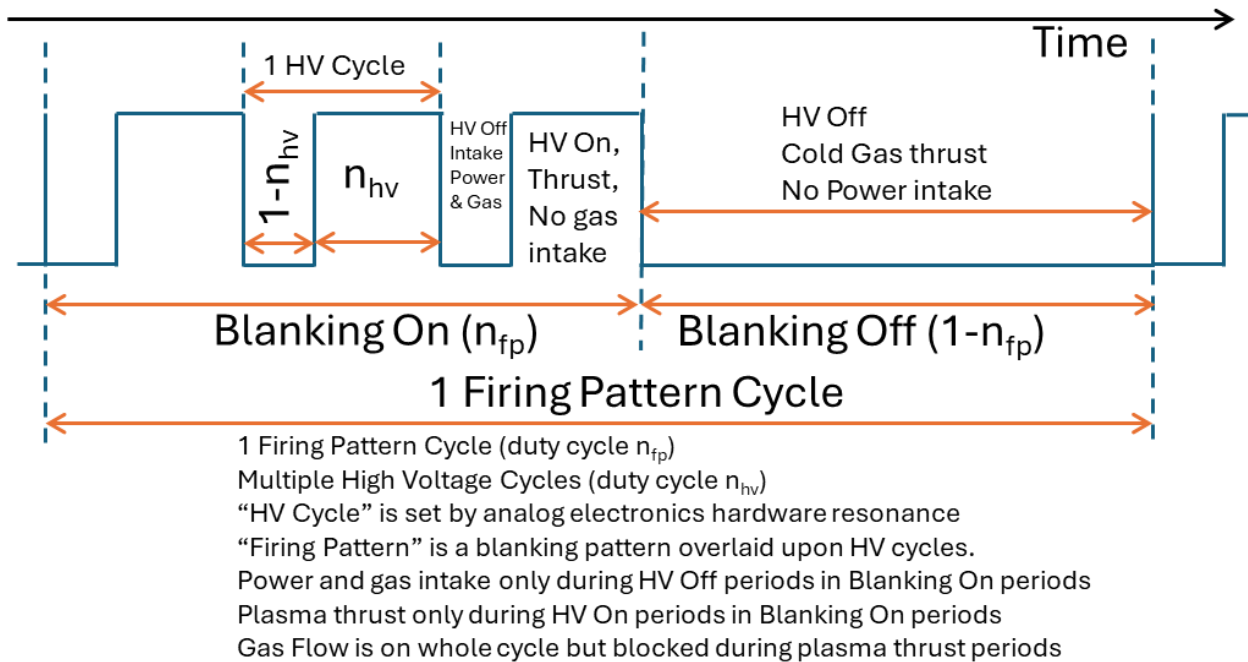


Figure 3 Operating cycle defined by high voltage pulses and blanking operations.

Energy is banked within capacitors during the power intake portions of the operating cycle. The total energy banked exceeds the total energy expended during the other portions of the cycle. Note that this assertion speaks to energy integrated over the cycle not to instantaneous power.

The fraction of the high voltage cycle where high voltage is present and energy is being expended is n_{hv} . The fraction of the high voltage cycle where high voltage is not present and energy is being drawn into the system is $1-n_{hv}$.

The fraction of the firing pattern where the high voltage cycle is permitted (including its off portion) is n_{fp} . The fraction of the firing pattern where no high voltage cycle is permitted, no energy is taken in, and no energy is expended is $1-n_{fp}$.

The total fraction of time in which energy is taken into the system is $n_{fp}*(1-n_{hv})$.

The total fraction of time in which energy is being expended and thrust created is $n_{fp}*n_{hv}$.

To account for pulsed operation, rates are integrated over an operating cycle to yield a scalar per cycle. Power is integrated to yield energy. Force is integrated to yield momentum. Mass flow rate is integrated to yield mass. All are in units per cycle. Given a cycle time, these are converted to average rate which is what most lab instruments report. A current sensor outputs a voltage that is proportional to the time average current flow. A thrust measurement system of a strain gauge (both spring-like and damper-like), the inertia of a large thruster mass, and a low pass filter amplifier produces an output voltage proportional to the time average thrust. A mass flow sensor using temperature sensors with their thermal mass and a low pass signal filter produces an output voltage proportional to the time average mass flow rate. To connect lab measurements to equation



values in this pulsed system, equation values are made time average values through the two-step process of converting to per cycle then to time averages.

A fraction, n_i , of neutral particles are ionized, yielding an electron and an ion. This is a single species model. Ionization requires energy. The same amount of energy is released during recombination, the inverse process. Recombination energy is released as kinetic energy of the new neutral molecule. The ionization energy of water vapor is 13.0 eV.

A fraction, n_{ae} , of electrons liberated by ionization are accelerated into the plume region by the potential difference on the acceleration grid.

A fraction, n_{ai} , of ions liberated by ionization are accelerated into the plume region by the potential difference on the acceleration grid and by attraction to the exhaust electrons that have left first. The acceleration grid potential is used for this model.

A fraction, n_{ti} , of ions liberated by ionization are trapped within the thruster due to the location of the potential energy peak. These ions collide with neutral molecules and the forward wall of the reaction chamber. (Note: the “forward wall” is in the direction of rocket movement, opposite the exhaust plume.)

As the plume ions recede, the trapped ions are eventually accelerated by the acceleration grid. The acceleration potential at that point in time is quite low due to the non-constant voltage applied to the acceleration grid by the power supply. This model assumes that the trapped ions have no power expended upon acceleration – i.e. that the acceleration potential voltage is zero for all trapped ions.

A fraction, n_{ri} , of ions liberated by ionization undergo recombination with free electrons while still within the reaction chamber. This is also the fraction of electrons liberated by ionization that undergo recombination.

All electrons liberated by ionization are either expelled into the plume or undergo recombination. The total of n_{ri} and n_{ae} is 1.0.

All ions liberated by ionization are expelled in the plume, or trapped within the thruster, or undergo recombination. The sum of n_{ai} , n_{ti} , and n_{ri} is 1.0.

Releasing an electron from a spark electrode requires an amount of energy called the Work Function. The amount of energy required is based upon the electrode material and surface properties. For stainless steel electrodes, the work function is 4.19 eV. Due to the pulsed operation, this model does not consider the reduction of work energy on stainless steel when presented with a continuous transverse electric field (an effect that, curiously, affects stainless steel and not most other metals).

Electrons released by one spark electrode are absorbed by another electrode. Electrons liberated during ionization are, in general, not absorbed by a spark electrode and rather remain within the plasma. These conditions ensure spacecraft neutrality.

Electrons released by an electrode generate additional electrons during ionization. These in turn, generate other ionizations and electrons. n_{ie} is the number of ionizations ultimately caused by a



single released electron. In the Townsend Avalanche portion of a spark, $n_{ie} > 1$. The Townsend 1st Ionization Coefficient, “ α ”, determines n_{ie} along with the spark gap, the electric field in the spark gap, and gas density in the spark gap. In [Ref.16], Sivos et al present curve fits of α for low current arcs in water vapor.

The Bernoulli equations for gas continuity are used to determine initial spark gap pressure and density from choke point dimensions and flow conditions.

Equations

Speed of sound, $v_{s,c}$, at the choke point depends upon water specific heat ratio ($\gamma=1.33$), universal gas constant R, vapor temperature, and water molar mass, M (0.0180158 kg/mol). T (°K) is the temperature of the water vapor, taken as equal to the temperature of the liquid/ice water from which it evaporated.

Equation 4 Speed of sound

$$v_{s,c} = \sqrt{\frac{\gamma RT}{M}}$$

The gas speed of sound and downstream plenum length set the amount of time needed for a spark cycle before information about the cycle can propagate to the upstream, non-choked flow, portion of the flowing vapor. Plenum minimum length, $d_{pl,min}$, is related to the speed of sound and the frequency of high voltage pulses, f_{hv} (which sets the minimum time available across the entire pulse cycle). A plenum length shorter than this would stop choked flow conditions and lower overall mass flow.

Equation 5 Plenum length constraint

$$d_{pl,min} = \frac{v_{s,c}}{f_{hv}}$$

For 20°C vapor and the thruster’s hardware-specific f_{hv} , minimum plenum length is 3.85 mm. Over the range -40 to 100°C, the largest minimum length is 4.36 mm. This is well below the actual plenum length of tens of mm, therefore downstream pulses do not affect choked flow conditions.

The Townsend 1st Ionization Coefficient, α , is used to determine n_{ie} , the number of ions formed from each electron released by a spark electrode. From [Ref.18] pg. 6, n_{ie} is related to α and the spark gap length, d_g :

Equation 6 Ionizations per Spark Electron

$$n_{ie} = e^{\alpha d_g}$$

In [Ref.16], Sivos et al teach that α is based upon the “reduced electric field” between electrodes in low-pressure water vapor. [Ref.16] Table 1 gives the curve fit parameters to calculate α/N from E/N (the “reduced electric field”) with E/N expressed in Townsend units (“Td” symbol). Here, N is the number density of neutral particles in the spark path, N_α . The electric field E is calculated from the acceleration voltage, V_a , and the spark gap, d_g .



The number density, N_α ($\#/m^3$), of gas at the downstream choked flow point is related to the mass flow, the mass of an individual neutral molecule m_n , the choked flow cross-section area A_c , and the gas speed $v_{s,c}$:

Equation 7 Gas number density

$$N_\alpha = \frac{\dot{m}_{meas}}{A_c v_{s,c} m_n}$$

The static pressure of neutral gas within the spark region immediately before a spark, p_{spark} , can be estimated using Bernoulli's relationship between pressure and velocity with constant temperature and density. This pressure is expected to match well with the Paschen curve of water vapor. For a spark potential of approximately 900V, the Paschen curve range for water vapor is 0.18 to 7.5 Torr cm.

Bernoulli's relationships show the interaction between conditions at the choked flow point (where static pressure, p_{choked} , is axiomatically zero) and the spark region, with its cross-section area A_{spark} for each of n_{th} thrust heads and gas at v_{spark} velocity initial velocity. Mass density is also required and is based upon numerical density.

Equation 8 Bernoulli Relations for Gas Properties at Spark Onset

$$A_c v_{s,c} = (A_{spark} n_{th}) v_{spark}$$

$$p_{spark} - p_{choked} = \frac{1}{2} (N_\alpha m_n) (v_{s,c}^2 - v_{spark}^2)$$

It is a constraint that the initial static pressure at the spark gap yields an achievable point within the water vapor Paschen curve given the available voltage. When dealing with vapor temperatures well above 25°C, the Paschen curve requires a temperature adjustment. The adjustment is outside the scope of this work.

The propellant mass used during a single cycle is the amount of cold gas used during the $(1-n_{fp})$ portion of the cycle, plus the gas flowing during the n_{fp} portion, itself split into a fraction that becomes plasma via spark and a fraction is expelled as cold gas just as in the $(1-n_{fp})$ portion. The term $n_{hv,cg}$ sets the split of the matter during the n_{fp} period. The mass flow here is the instantaneous peak mass flow from the downstream plenum into the reaction region. The number of neutrals can be determined by dividing any mass by m_n , the mass of a single neutral water molecule.

Equation 9 Model Mass Flow Equations

$m_{cycle} = m_{hv} + m_{hv,cg} + m_{cg}$	(a)	Spark formation causes shock waves that interfere with incoming neutrals, causing mass flow to be zero during the n_{hv} portion of the cycle, itself only during the n_{fp} portion of the cycle.
$m_{hv} = \dot{m} \left(\frac{n_{fp}(1-n_{hv})}{f_{cycle}} \right) (1-n_{hv,cg})$	(b)	
$m_{hv,cg} = \dot{m} \left(\frac{n_{fp}(1-n_{hv})}{f_{cycle}} \right) n_{hv,cg}$	(c)	
$m_{cg} = \dot{m} \left(\frac{1-n_{fp}}{f_{cycle}} \right)$	(d)	



<p>Unit checks: Kg/cycle=kg/cycle + kg/cycle kg/cycle=kg/s * s/cycle</p>		<p>m_{hv} is the amount of matter available during the plasma portion of a cycle. $m_{hv,cg}$ is the amount of matter that leaves the system before it can be used by the plasma portion of the cycle. m_{cg} is the amount of matter available during the non-plasma portion of a cycle. Measured mass flow is the time average flow.</p>
--	--	---

Energy imparted to accelerated electrons and ions comes from the accelerating electrodes. A measurement, V_{meas} , of the potential across the electrodes is a RMS average of the peak potential, V_a , due to the circuitry within handheld meters able to measure this voltage directly without a voltage divider circuit. Being singly charged, the energy conveyed by the field is related to q , the elementary charge, and the acceleration potential. Ion and electron velocities are calculated from the energy input.

Equation 10 Model velocities

$V_a = \frac{V_{meas}}{\sqrt{n_{hv}n_{fp}}}$ $qV_a = \frac{1}{2}m_e v_e^2$ $qV_a = \frac{1}{2}m_i v_i^2$ $q(0) = \frac{1}{2}m_i v_{ti}^2 = 0$	<p>(a)</p> <p>(b)</p> <p>(c)</p> <p>(d)</p>	<p>Acceleration voltage is related to the measured voltage by an RMS average due to the averaging circuits within volt meters. (Empirically confirmed for Fluke meters used to measure the high voltage directly without use of a voltage divider.) Accelerated electrons and ions get their kinetic energy from the voltage across the acceleration grid. Unit charge, q, is used for each species. Trapped ions leave under a zero-voltage condition, so their exit velocity is only thermal and taken as an average of 0.</p>
---	---	---

Power is required to pressurize and flow a gas. The volume rate, Q (m^3/s), swept by flowing gas depends upon its bulk velocity, v_{ex} , and the area, A , moved through. The power required, P_g , to flow some volumetric flow rate, Q , of gas at pressure dp is:

Equation 11 Energy of pressurized flowing gas

$P_g = Q dp$ $Q = v_{ex}A$ $P_g = v_{ex}A dp$	<p>(a)</p> <p>(b)</p> <p>(c)</p>	<p>Flowing, pressurized gas is related to power. Flowing gas is related to bulk velocity and exit area.</p>
---	----------------------------------	---



Energy is consumed within a cycle in several ways:

- Energy is used to accelerate electrons, forming the virtual cathode.
- Energy is used to accelerate some ions.
- Energy is needed to release electrons from the spark electrodes.
- Energy is needed to ionize gas. Some of that is recovered and becomes energy used to pressurize and flow gas.
- $E_{\text{cycle,ir}}$ is the remaining energy expended for ionization that was not recovered.

Note that power terms, such as flowing pressurized gas, are converted to energy values by using the timespan during which they occur.

The bulk velocity of the pressurized flowing gas must allow it to traverse the distance from inlet to exhaust plane, d_{gas} , within each cycle.

Equation 12 Model energy uses

$E_{\text{cycle}} = E_{\text{cycle,ae}} + E_{\text{cycle,ai}} + E_{\text{cycle,g}} + E_{\text{cycle,spark}} + E_{\text{cycle,ir}}$	(a)	Define the energy sinks during a cycle.
$E_{\text{cycle,ae}} = \frac{1}{2} \left(\frac{m_{\text{hv}}}{m_n} n_i n_{\text{ae}} m_e \right) v_e^2$	(b)	Energy is used to accelerate electrons, forming the virtual cathode.
$E_{\text{cycle,ai}} = \frac{1}{2} \left(\frac{m_{\text{hv}}}{m_n} n_i n_{\text{ai}} m_i \right) v_i^2$	(c)	Energy is used to accelerate some ions.
$E_{\text{cycle,g}} = \left(\frac{n_{\text{fp}} n_{\text{hv}}}{f_{\text{cycle}}} \right) v_{\text{ex}} A dp$	(d)	Energy is needed to release electrons from the spark electrodes.
$E_{\text{cycle,spark}} = \left(\frac{m_{\text{hv}}}{m_n} n_i \right) \left(\frac{1}{n_{\text{ie}}} \right) W_e$	(e)	Energy is needed to ionize gas. Some of that is recovered and becomes energy used to pressurize and flow gas.
$E_{\text{cycle,ir}} = \left(\frac{m_{\text{hv}}}{m_n} n_i E_i - \left(\frac{n_{\text{fp}} n_{\text{hv}}}{f_{\text{cycle}}} \right) v_{\text{ex}} A dp \right)$	(f)	$E_{\text{cycle,ir}}$ is the remaining energy expended for ionization that was not recovered.
$\frac{m_{\text{hv}}}{m_n} n_i E_i \geq \left(\frac{n_{\text{fp}} n_{\text{hv}}}{f_{\text{cycle}}} \right) v_{\text{ex}} A dp$	(g)	The bulk velocity must be great enough for the pressurized gas to transit from inlet to exit point during each cycle.
$v_{\text{ex}} \geq d_{\text{gas}} f_{\text{cycle}}$	(h)	



Ionization energy recovered by recombination is the source of pressurization and flow energy. This relates pressure thrust to mass flow.

Equation 13 Model recombination energy

$\frac{m_{hv}}{m_n} n_i n_{ri} E_i = \left(\frac{n_{fp} n_{hv}}{f_{cycle}} \right) v_{ex} A dp$ <p>Unit checks: Kg/cycle/kg*ion/#*recov_ions/ion#*J/ion = J/cycle m/s*m^2*N/m^2*s/cycle=Nm/s=J/s* s/cycle = J/cycle</p>	(a)	Ionization energy recovered by recombination is the source of pressurization and flow.
--	-----	--

The average current of a spark through a single thrust head is a useful tool for assessing reasonableness. Sparks are a well-studied phenomena with expectations set for apparent spark energy relative to current. The numerator in the following equation gives the charge released from a single electrode in a system consisting of n_{th} thrust heads. The denominator gives the total time in which the charge flows.

Equation 14 Model average spark current

$$I_{spark} = \frac{\left(\frac{m_{hv}}{m_n} n_{th} n_i \right) \left(\frac{q}{n_{ie}} \right)}{\left(\frac{n_{hv} n_{fp}}{f_{cycle}} \right)}$$

Momentum is generated within a cycle in several ways. As the mechanisms don't occur at the same time, totalizing them as momentum permits time average force to be determined and related to measurements.

- Accelerating electrons gives momentum.
- Accelerating ions gives momentum.
- Pressurized gas leaving gives momentum.
- Bulk mass flow gives momentum.
- Cold gas bulk flow gives momentum, moving at the speed of sound at the choke point and having no pressure effects.

Equation 15 Model momentum sources

$\rho_{cycle} = \rho_{cycle,ae} + \rho_{cycle,ai} + \rho_{cycle,g}$ $+ \rho_{cycle,m} + \rho_{cycle,cg}$ $\rho_{cycle,ae} = \left(\frac{m_{hv}}{m_n} n_i n_{ae} m_e \right) v_e$ $\rho_{cycle,ai} = \left(\frac{m_{hv}}{m_n} n_i n_{ai} m_i \right) v_i$	(a) (b) (c)	Define the sources of momentum during each cycle. Accelerating electrons gives momentum. Accelerating ions gives momentum. Pressure gives momentum.
--	-----------------------	--



$\rho_{cycle,g} = \left(\frac{n_{fp} n_{hv}}{f_{cycle}} \right) A dp$ $\rho_{cycle,m} = (m_{hv} n_i n_{ri}) v_{ex}$ $\rho_{cycle,cg} = (m_{cg} + m_{hv,cg}) v_{s,c}$ <p>Unit checks: Kg/cycle*(#/kg)*(ion/#)*(accel_elec/ion)* (kg/elec)*(m/s) = (kg/cycle) * (m/s) = Ns/cycle</p>	<p>(d) (e) (f)</p>	<p>Bulk mass flow gives momentum. Cold gas bulk flow gives momentum, moving at the speed of sound at the choke point and having no pressure effects.</p>
---	----------------------------	--

When the pressurized gas pressure, dp, exceeds the vapor pressure of water vapor, the gas is modeled as being heated because no observation of phase change back to liquid water have been observed. The temperature, T_{dp} (°K), needed to maintain water vapor at the dp pressure is used in the Arden Buck equation for water vapor pressure ([Ref.2]):

Equation 16 Water vapor pressure

$$dp = 611.21 e^{[(18.678 - \frac{(T_{dp} - 273.15)}{234.5}) (\frac{(T_{dp} - 273.15)}{257.14 + (T_{dp} - 273.15)})]}$$

Tested thrusters have used thermoplastic reaction chambers and overserved no melting or discoloration due to thermal damage. These observations imply T_{dp} is low, well below the melting point of the plastic.

The various fractions and variables have acceptable ranges for the model to make physical sense.

Equation 17 Model constraints

$0 < n_{hv} \leq 1$ $0 < n_{fp} \leq 1$ $0 \leq n_i \leq 1$ $0 \leq n_{ai} \leq 1$ $0 \leq n_{ae} \leq 1$ $0 \leq n_{ri} \leq 1$ $0 \leq n_{ti} \leq 1$ $0 \leq n_{hv,cg} \leq 1$ $0 \leq dp$ $n_{ai} + n_{ri} + n_{ti} = 1$	<p>(a) (b) (c) (d) (e) (f) (g) (h) (i) (j)</p>	<p>Define ranges for fractions and some values that cannot be negative (such as pressure).</p>
--	--	--



There are relationships between the amount of electrons expelled, the amount of ions expelled, and the amount of ions that are trapped by a net pressure due to repulsion from nearby plume ions.

Equation 18 Model plume allocations

$n_{ae} + n_{ri} = 1$ $n_{ae} = n_{ai} + n_{ti}$ $n_{ti} \leq n_{ai}$ $0 < n_{ai}$	<p>(a) (b) (c) (d)</p>	<p>There is one electron liberated by each ionization.</p> <p>All electrons liberated by ionization are either expelled by acceleration or undergo recombination.</p> <p>The fraction of expelled electrons is the combined amount of expelled ions, either through acceleration or eventual release of trapped ions.</p> <p>There are no more trapped ions than those that are accelerated, otherwise the trapped ions would simply leave.</p> <p>Some ions are accelerated, otherwise no electrons would be trapped and there would be no physical evidence that is observed of ion implantation as well as simulation results of trapped ions colliding with the front wall.</p>
--	------------------------------------	---

Measurements of power, thrust, and mass flow are related to the per-cycle values as:

Equation 19 Model observation relations

$P_{meas} = E_{cycle} f_{cycle}$ $F_{meas} = \rho_{cycle} f_{cycle}$ $\dot{m}_{meas} = m_{cycle} f_{cycle}$ <p>Unit checks: $J/s = (J/cycle) * (cycle/s)$ $N = (Ns/cycle) * (cycle/s)$ $kg/s = (kg/cycle) * (cycle/s)$</p>	<p>(a) (b) (c)</p>	<p>Measured power relates to cycle frequency and energy per cycle.</p> <p>Measured thrust relates to cycle frequency and momentum per cycle.</p> <p>Measured mass flow relates to cycle frequency and mass per cycle.</p>
--	----------------------------	---

Efficiencies

A typical measure of electric propulsion efficiency is the ratio of beam kinetic power to input electrical power. The constituents in this model would be $E_{cycle,ae}$ and $E_{cycle,ai}$ for electron and ion beam kinetic energies respectively. This measure of efficiency carries the assumption that propulsion occurs primarily from the beam kinetic energy, an assumption that is only valid in the derivative case of no pressure component of thrust. However, for the sake of comparison, beam power efficiency, η_{beam} , is related to energy for accelerating particles, cycle frequency, and measured input power:



Equation 20 Beam power efficiency

$$n_{beam} = \frac{f_{cycle}(E_{cycle,ae} + E_{cycle,ai})}{P_{meas}}$$

The model expects most thrust to come from the pressure term. Thus, electrical efficiency, n_E , is the portion of the electrical energy used to generate the pressure term.

Equation 21 Electrical energy efficiency

$$n_E = \frac{E_{cycle,g}}{E_{cycle}}$$

Mass utilization efficiency, n_{mass} , is based upon the amount of matter used within the propulsive period:

Equation 22 Mass utilization efficiency

$$n_{mass} = \frac{m_{hv}}{m_{cycle}}$$

The ratio of thrust to power, n_{tp} (N/W), is:

Equation 23 Thrust to power ratio

$$n_{tp} = \frac{\rho_{cycle}}{E_{cycle}}$$

3.2 Equation Solving

The preceding model has more unknowns than measured values (at least in present experiments). Solutions can be found by numerical search algorithms, looking for parameter combinations that best match the observations without violating constraints. Given the interactions between values, the model can be solved by searching for the following parameters and calculating the remaining parameters from these and observations:

- n_{ai} – fraction of ions that accelerated
- n_{ri} – fraction of ions that are recombined, creating pressurized neutral gas
- n_i – fraction of neutrals that are ionized
- dp – pressure of created neutral gas
- v_{ex} – bulk flow velocity of pressurized neutral gas
- \dot{m} – mass from the downstream plenum into the reaction region
- $n_{hv,cg}$ – portion of mass in the n_{fp} firing regime that becomes cold gas instead of plasma



For background, the arrangement of software for finding solutions is shown below:

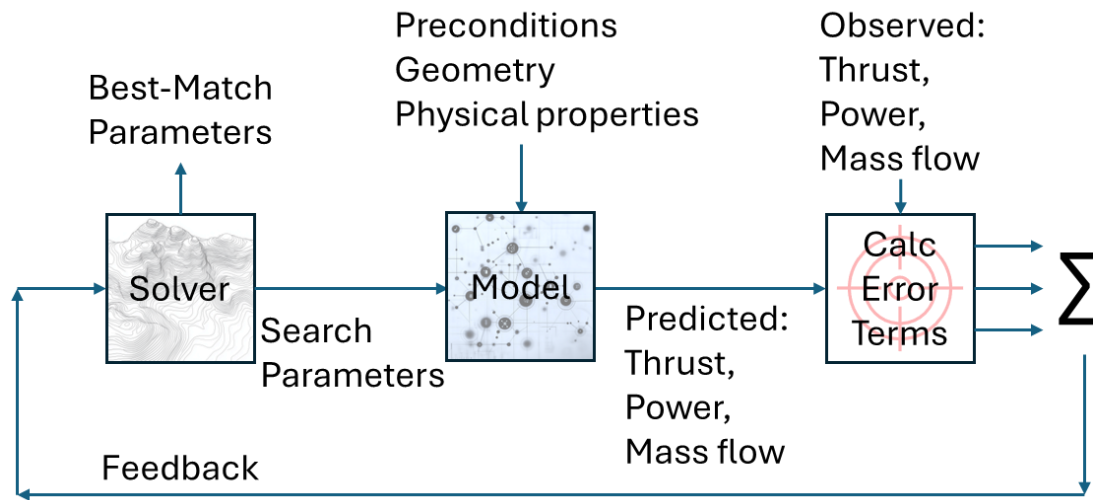


Figure 4 Model solver software architecture

A “solver” is the set of algorithms that attempt to find parameter sets that satisfy constraints while also being excellent solutions to the unknowns. The “model” is a set of equations that combines the search parameters with physical details to predict key values. The predicted values are compared to the observed values and an error determination made for each. The solver uses the combined total error as feedback to guide its search.

The error terms are normalized to the absolute fraction of prediction difference from observations for thrust, power, and mass flow. A prediction of zero thrust, zero power, and zero mass flow would yield an error score of 3.0, being perfectly incorrect in each of the observed quantities. The formula for the error for a single prediction is shown below. It is linear for predictions near the observation and non-linear elsewhere. The formulation has been shown to accelerate solver convergence. The formulation is applied to each prediction/observation and the score summed.

Equation 24 Model error term formulation

$$f = \frac{|Prediction - Observation|}{Observation}$$

$$score = \begin{cases} f, & f \leq 1 \\ f^2, & f > 1 \end{cases}$$

All results presented in this paper come from parameters that satisfy the model constraints (such as no over unity energy components) and make predictions that match observations to within parts-per-million error (i.e. to tolerances better than available with instrumentation).

Parameters will vary with the final search score. Thus, parameters are presented for best and worst solutions that still fit constraints.



4. In-Space Test Results 2024-09

4.1 Poseidon™ Thruster Model M1.5

The M1.5 thruster has 5 thrust heads in a linear arrangement along the diagonal face of a 1U device that includes propellant. The device includes 2 valves (in series per rideshare safety), a CPU (> 20kRad TID tolerance), and power conversion circuits. Specifications are:

Parameter	Value
Dimensions	95 x 95 x 95 mm
Mass	1020g wet 770g dry
Propellant	Liquid water, 250g
Power input	12-18V (15V nominal) 2A safety limit 1.5W typical 9-pin MicroD connector
MEOP	15.2 psi
Communication interface	RS-485 Half Duplex, 2-wire
Thrust	37.49 mN
I_{sp}	4,800 sec
Materials	Aluminum Low-outgassing plastic FR-4 circuit board

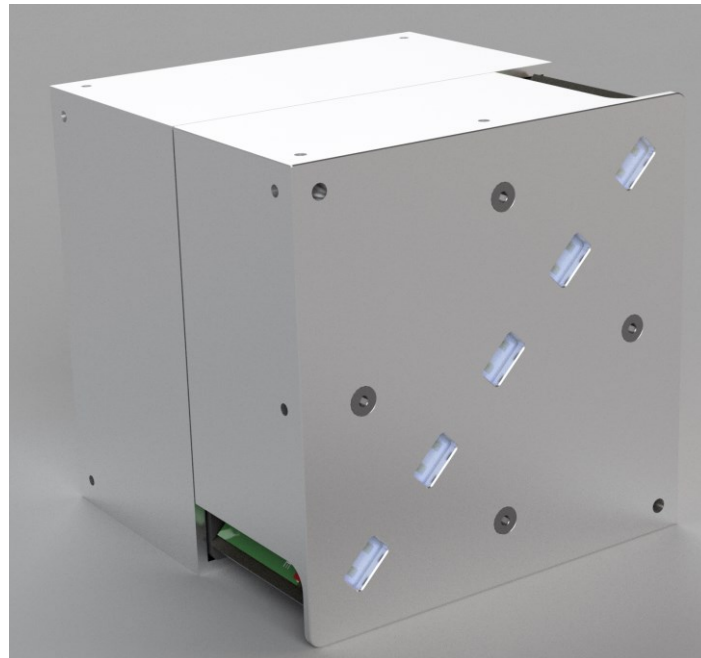


Figure 5 Rendering of Model M1.5 thruster.



4.2 Setup and Results Summary

A Model M1.5 thruster is rigidly mounted onto a larger satellite owned by a third-party, with a total mass in the 100-200 kg range. The thruster was fueled with 250g of liquid water. The satellite was on the SpaceX Transporter 11 mission, launched on Aug 24, 2024. The thruster was tested in space on Sep 11, 2024.

The device results were:

- 37.49 mN thrust (average) (7.49 mN/thrust head)
 - Cold gas thrust is $\leq 0.9\%$ of total thrust
- 1.49 W input low voltage electrical power (average, limited to $\leq 2A$ instantaneous by hardware fuse)
 - < 1.0 W high voltage power delivered to plasma production and acceleration
- $\geq 4,800$ sec Isp (average, based on choked flow limit of maximum gas flow rate)
- 3.84 degrees off-boresight thrust angle (compared to 6.2 degrees predicted by simulation)

During the test, the thruster was fired for 5 minutes continuously then powered off. Before and after the 5-minute period, no electrical energy was flowing to the thruster. That is, the thruster was not merely in an “idle” or “standby” mode. The timing behavior was set by the satellite operator’s flight computer.

The satellite operator made measurements of:

- Input voltage
- Input current
- Craft 3-axis angular velocities

The satellite operator computed:

- Craft Center of Gravity before firing in the craft body reference frame
- Craft Moment of Inertia before firing
- Thruster location and orientation in the craft body reference frame

Thrust is computed from rotational acceleration and torque, derived from angular velocities and geometry. Craft rotation was chosen because an orbit change could not be undone with certainty due to lack of another thruster on the craft and the experimental nature of the tests.

Mass flow is passive in the tested M1.5 device. No propellant heater, mass flow controller, or mass flow rate sensor are present in the system. Mass flow is taken from choked flow calculations.

The bus power provided was 1.49 W average. Accounting for onboard electronics power usage and conversion efficiencies, 0.993 W average was delivered as high voltage to make and accelerate plasma.

In-flight craft data is not publicly available here due to contractual restrictions.



5. Ground Test Results at Miles Space

5.1 Setup and Results Summary

In [Ref.8], Tsifakis et al teach the successful use of a strain gauge to measure small thrust values. Strain gauges are found to have superior zero-drift behavior compared to laser interferometer methods. Tsifakis also demonstrates success with a suspended thruster, rather than flexure-based inverted pendulum systems. The combination of these permits a small, economical thrust stand system. The thrust stand used at Miles Space is based upon Tsifakis' success.

The thrust stand system used at Miles Space is shown schematically in the figure below. The thruster is attached to a level stage, itself suspended from a rigidly mounted frame by 4 wires. Lateral thrust is measured using a strain gauge. Microslips at the point of contact between the strain gauge's set screw and the thruster body, as well as twisting by a vectored thrust or tests of a linear array of thrust heads, is reduced by introducing a 2D linearization plate that is attached to the set screw. The linearization plate ensures there is a line of contact with the thruster, not a simple point.

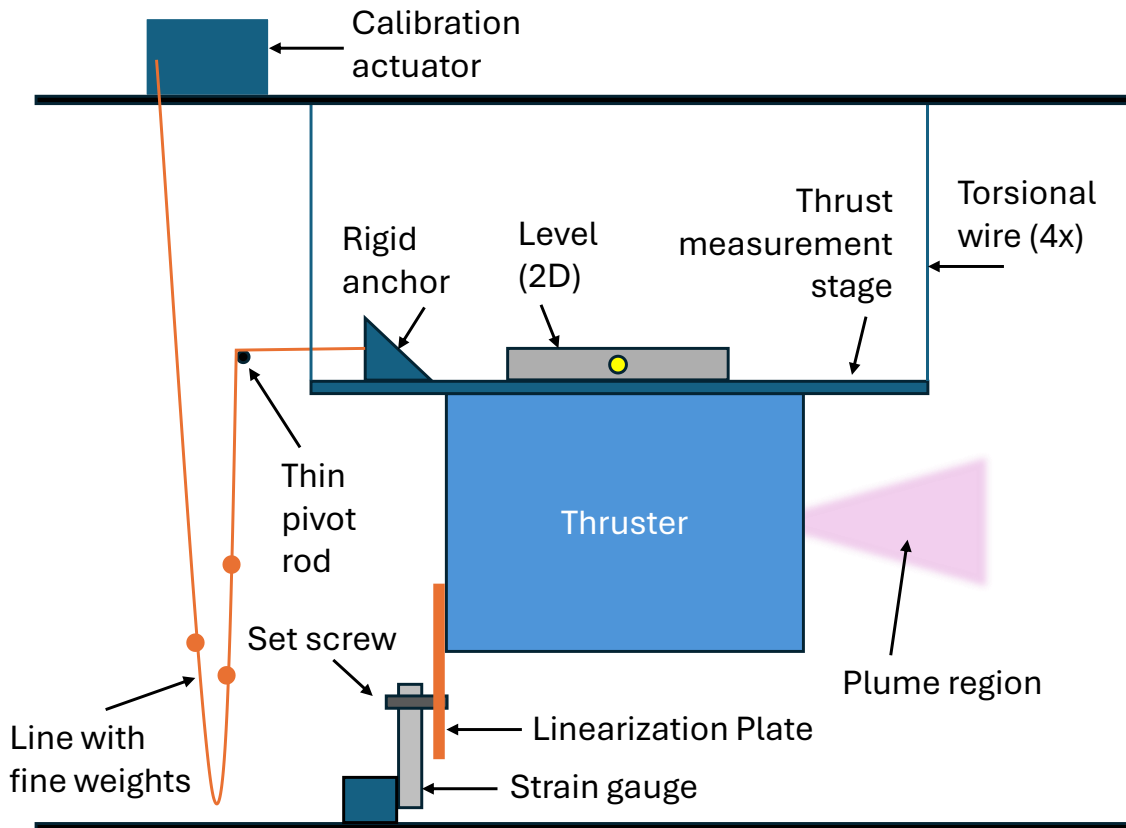


Figure 6 Thrust stand configuration at Miles Space



Calibration is done by adding lateral force upon the thrust measurement stage. Lateral force comes from an industry-typical arrangement of weights upon a fine line, allowed to flex over a thin, low-friction pivot point, and with the line being adjusted by an actuator motor. The “calibration pyramid” protocol is used in which weights are added in sequence and removed in sequence, such that each weight’s effect is measured in separate periods, permitting zero-drift determination.

An instrumentation amplifier is used to amplify the strain gauge signal. The amplifier output has an analog low pass filter attached. Thrust is determined from the digitized value of this voltage and calibration results expressed as mN/V.

The mass flow sensor’s output voltage is directly connected to the data acquisition system. I_{sp} is calculated from this signal and the thrust.

Input electrical voltage is measured by the data acquisition system. Input current flows through a Hall Effect current sensor that produces an output voltage linearly related to the current flowing through it. The current sensor’s output voltage is directly connected to the data acquisition system. Input electrical power is calculated as the product of DC voltage and current.

Signals are connected to a data acquisition system. Data is collected at 100Hz, though this can be varied per experiment. Analog data is post processed using a low pass filter from the Python scipy software package. The filter is a 4th order Butterworth low pass filter. For strain gauge movement, 2Hz is the critical frequency. For voltage, current, vacuum chamber pressure, and mass flow, 1Hz is the critical frequency. Filtered values are used for time-series analysis. Unfiltered values are used for frequency analysis.

Live filtering, including moving average, introduces phase delays in data and makes temporal correlations challenging (especially with boolean signals that do not merit filtering). Post-processing filtering is done using the Python function `scipy.signal.filtfilt` (and newer version `sosfiltfilt`). From [Ref.9], this function performs a linear digital filter forward and backward, with a zero-phase shift and a filter order twice that of the original. Compared to moving average filtering (common in this author’s experience and used in [Ref.8]), the signal is cleaner and better suited for causal analysis due to the lack of phase delay. See [Ref.9] for further reading on the issues with the use of a moving average filter.

Typical calibration and experiment results are shown in the following sections, with values of:

- 29 mN average thrust, 0.8 W input low voltage power, 2,750 sec I_{sp}
- 37 mN average thrust, 1 W input low voltage power, 3,250 sec I_{sp}

The lab mass flow system is passive, relying upon water vaporization in vacuum. There is experimental evidence that the current mass flow system is delivering too much mass, showing signs of increasing thrust with decreasing mass flow. As such, the I_{sp} values measured herein may be too low.

There is a known ground loop issue that occurs when mass flow valves are activated in the thrust stand. The solid-state relay used causes a small, constant voltage shift on the data acquisition system. The result is that the cold gas thrust is overstated in the strip charts shown in this paper.



Calibrations done during other experiment firings show the mN/V calibration factor is unaffected by this shift and that the plasma thrust deflection from cold gas is still valid.

5.2 Typical Calibration #202405080900

This experiment is done on Miles Space’s thrust stand. It performs a calibration operation in which known masses are incrementally added and removed as lateral force proxies on the thrust stand.

The following graphs show the strain gauge voltage over time as the test masses are loaded and unloaded. Note that the test masses deflect the strain gauge well beyond the noise band.

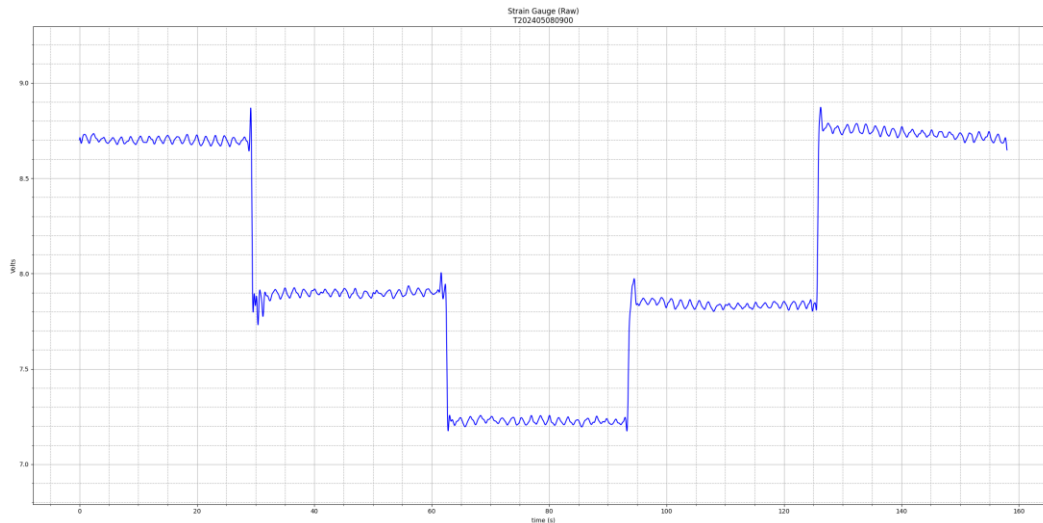


Figure 7 Calibration 202405080900 strain gauge response

5.3 Typical Experiment #T202405081004

This experiment is done on Miles Space’s thrust stand and uses “Stick 10” from a recent manufacturing lot of thrust heads. The device being tested has 5 thrust heads in a linear arrangement. Water vapor is the propellant. Average thrust is 29.6 mN, 0.8 W input low voltage power, 2,800 sec Isp over a 3-minute firing duration.

After a valid calibration, the test cycle is:

- Unpowered idle period of 30 seconds to establish sensor baselines.
- Open mass flow and do 30 seconds of unpowered, cold gas flow.
- Power-on the thruster for 3 minutes.
- Turn off the thruster and do 30 seconds of unpowered, cold gas flow.
- Turn off mass flow and do unpowered idle period for 30 seconds.

The following graphs show data for thrust and mass flow. Mass flow raw data is shown, unconverted to engineering units, to show natural sensor noise and the effect of the backflow pulses on the mass flow. The thrust graph shows firing data is well outside the noise band of idle or cold gas readings. The mass flow graph shows the firing region backflow as increased variation in flow.

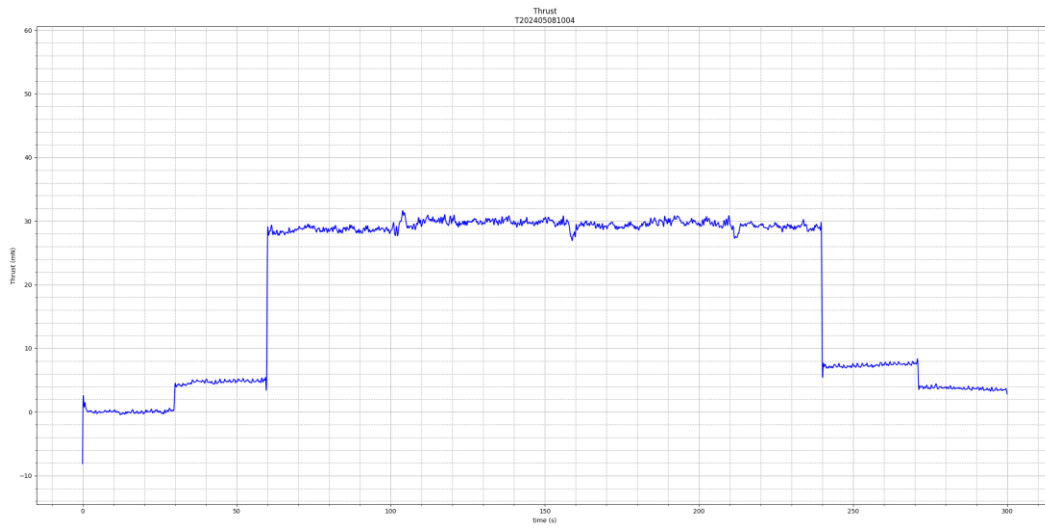


Figure 8 Experiment 202405081004 thrust

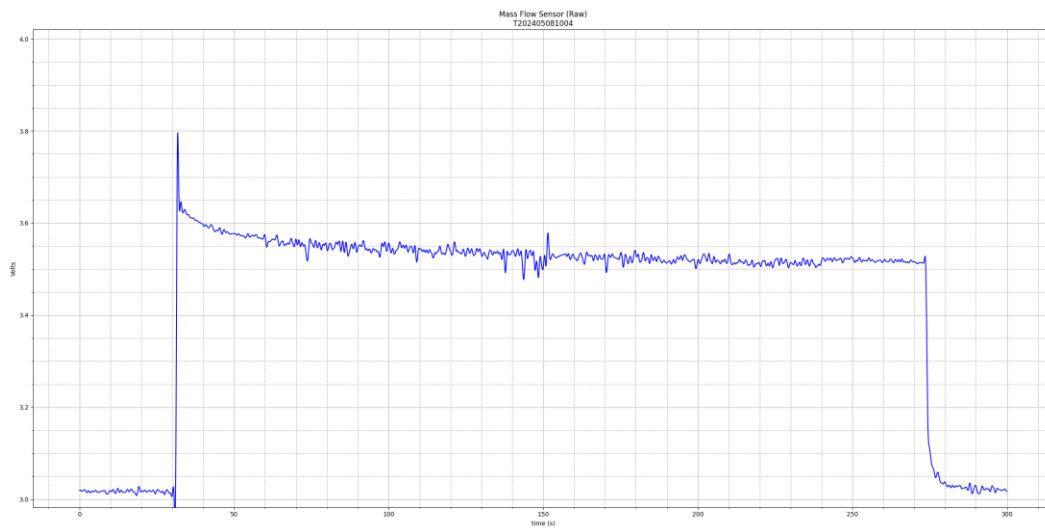


Figure 9 Experiment 202405081004 raw mass flow sensor reading



5.4 Typical Experiment #T202405151412

This experiment is done on Miles Space’s thrust stand and uses “Stick 11” from a recent manufacturing lot of thrust heads. The device being tested has 5 thrust heads in a linear arrangement. Water vapor is the propellant. Average thrust is 37 mN, 1 W input low voltage power, 3,274 sec Isp over a 3-minute firing duration.

After a valid calibration, the test cycle is:

- Unpowered idle period of 30 seconds to establish sensor baselines.
- Open mass flow and do 30 seconds of unpowered, cold gas flow.
- Power-on the thruster for 3 minutes.
- Turn off the thruster and do 30 seconds of unpowered, cold gas flow.
- Turn off mass flow and do unpowered idle period for 30 seconds.

The following graphs show data for thrust and mass flow. Mass flow raw data is shown, unconverted to engineering units, so as to show natural sensor noise and the effect of the backflow pulses on the mass flow. The thrust graph shows firing data is well outside the noise band of idle or cold gas readings. The mass flow graph shows the firing region backflow as increased variation in flow.

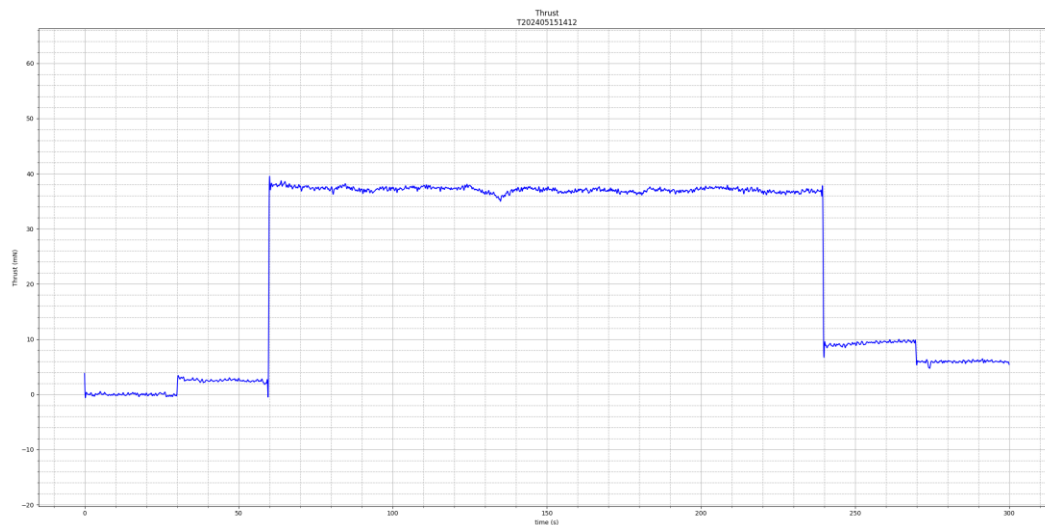


Figure 10 Experiment 202405151412 thrust

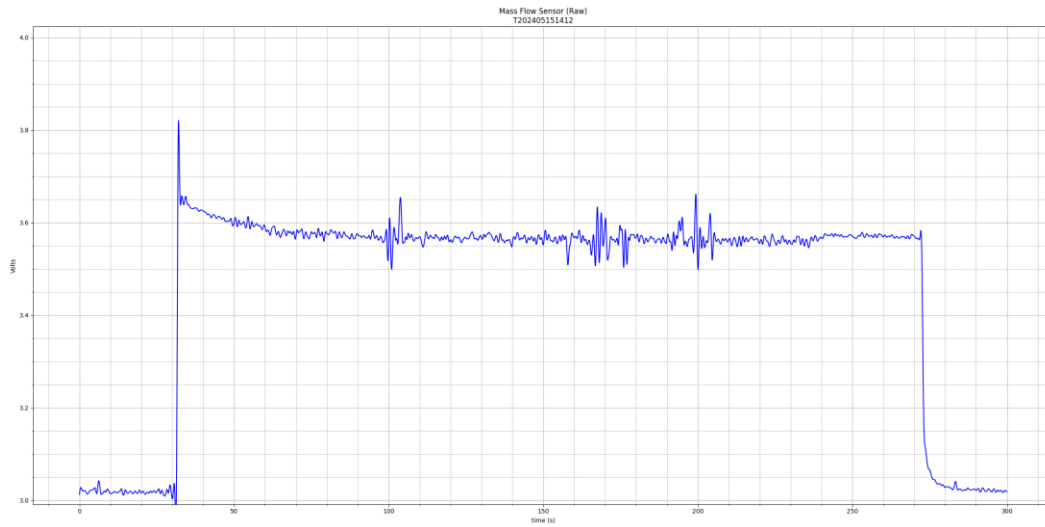


Figure 11 Experiment 202405151412 raw mass flow sensor reading

6. Model Results

6.1 Model Results for In-Space Test

Model equation solutions are presented here for the In-Space Test Results 2024-09. The results are compared to physical expectations to test validity.

Solution Case: In-Space Test Results 2024-09

Observations	Units	Value
Thrust	mN	37.49
Power (high voltage)	W	0.993
Mass Flow	ug/s	783

Preconditions	Units	Value
Water temperature	C	20
Vapor pressure	Pa	2,338
Voltage	V	967
Spark Paschen pd	Torr cm	5.03
n_{ie}	#/electron	38,844
Ion accel velocity	m/s	101,787
Electron accel velocity	m/s	18,440,706



Solution Quality	Units	Best	Worst	Avg
Sum(Abs(Error)/Meas)	ppm	0.0007	0.0898	0.0245
Constraints met?		Yes		

Efficiencies	Units	At Best	At Worst	Avg	Min	Max
n_{beam}	%	55.3%	13.8%	48.1%	0.0%	58.3%
n_E	%	44.3%	86.1%	51.6%	41.3%	100.0%
n_{mass}	%	5.6%	5.7%	5.7%	5.3%	6.1%
Thrust:Power ratio	mN/W	37.8				
I_{sp}	sec	4,880				

Energy Usage	Units	At Best	At Worst	Avg	Min	Max
E_{cycle}	J/cycle	1.49E-03	1.49E-03	1.49E-03	1.49E-03	1.49E-03
$E_{cycle,ae}$	%	29.724%	7.306%	27.940%	0.008%	38.450%
$E_{cycle,ai}$	%	25.599%	6.481%	20.121%	0.007%	29.055%
$E_{cycle,g}$	%	44.277%	86.113%	51.564%	41.294%	99.984%
$E_{cycle,spark}$	%	0.000%	0.001%	0.000%	0.000%	0.001%
$E_{cycle,ir}$	%	0.400%	0.098%	0.376%	0.000%	0.517%
I_{spark}	A	6.06E-07	1.17E-06	7.04E-07	5.65E-07	1.36E-06

Thrust Sources	Column1	At Best	At Worst	Avg	Min	Max
ρ_{cycle}	Ns/cycle	5.62E-05	5.62E-05	5.62E-05	5.62E-05	5.62E-05
$\rho_{cycle,ae}$	%	0.000%	0.000%	0.000%	0.000%	0.000%
$\rho_{cycle,ai}$	%	0.013%	0.003%	0.010%	0.000%	0.015%
$\rho_{cycle,g}$	%	99.150%	99.160%	99.154%	99.146%	99.161%
$\rho_{cycle,m}$	%	0.000%	0.001%	0.000%	0.000%	0.001%
$\rho_{cycle,cg}$	%	0.837%	0.836%	0.836%	0.832%	0.839%
v_{ex}	m/s	11.82	22.99	13.77	11.03	26.70
dp	Pa	2,564	2,564	2,564	2,563	2,564
T_{dp}	C	21.49	21.49	21.49	21.49	21.49
$T_{dp}-T$	C	1.49	1.49	1.49	1.49	1.49



Mass Usage	Units	At Best	At Worst	Avg	Min	Max
m_{cycle}	ug/cycle	1.18	1.18	1.18	1.18	1.18
m_{hv}	%	5.592%	5.654%	5.734%	5.310%	6.102%
$m_{\text{hv,cg}}$	%	0.511%	0.449%	0.370%	0.001%	0.793%
m_{cg}	%	93.897%	93.897%	93.897%	93.897%	93.897%

Allocations	Units	At Best	At Worst	Avg	Min	Max
n_i	fraction	0.1453	0.2774	0.1653	0.1244	0.3425
n_{ae}	fraction	0.0089	0.0011	0.0078	0.0000	0.0124
n_{ai}	fraction	0.0077	0.0010	0.0056	0.0000	0.0094
n_{ri}	fraction	0.9911	0.9989	0.9922	0.9876	1.0000
n_{ti}	fraction	0.0012	0.0001	0.0022	0.0000	0.0061
$n_{\text{hv,cg}}$	fraction	0.0837	0.0736	0.0606	0.0001	0.1300

The first check is that constraints are met and that the score is acceptably low. The “Solution Quality” section above shows constraints met and the worst solution is <0.1 ppm total difference from observation. This is quite acceptable.

The spark is initiated under the condition of 5.03 Torr cm which is well within the range of the water vapor Paschen curve which is 0.18 to 7.5 Torr cm with approximately 900V available to form a spark, shown below from [Ref.16] Figure 2:

J. Phys. D: Appl. Phys. **48** (2015) 424011

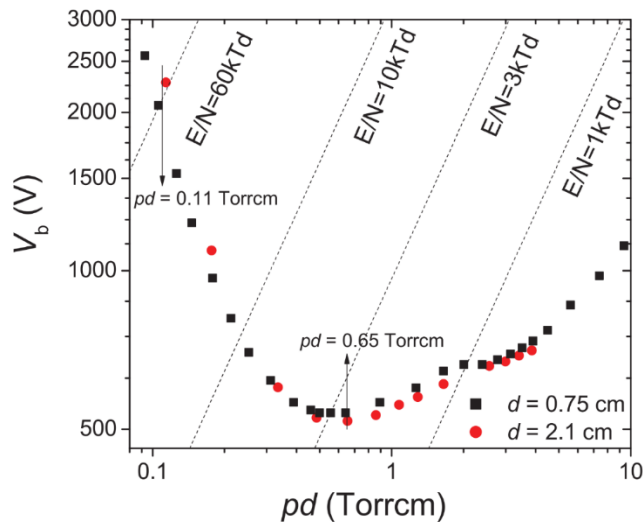


Figure 12 Water vapor Paschen curve. From [Ref.16] Figure 2.



The model shows about 55% of the input power becomes kinetic energy in the beam. About 44% of the input power is expended on propulsion (pressurization).

5.592% of neutral gas is available for ionization. Of this, 14.5% are ionized by sparks. Of ions, 99.11% will recombine and become pressurized neutrals with a pressure of 2,564 Pa, a bulk exit velocity of 11.8 m/s, and a temperature rise of 1.5C. 0.77% of ions are accelerated into the beam. 0.89% of electrons are accelerated into the beam. 0.12% of ions are trapped on the interior portion of the potential energy hill.

Mass is mostly expelled as cold gas, 93.9% + 0.511% being cold gas.

The spark current is $6e-7$ Amps (0.6 uA) which is in the Townsend dark-discharge regime. Thus, spark operation may not be visible. From [Ref.19], spark behavior over many decades of currents is shown:

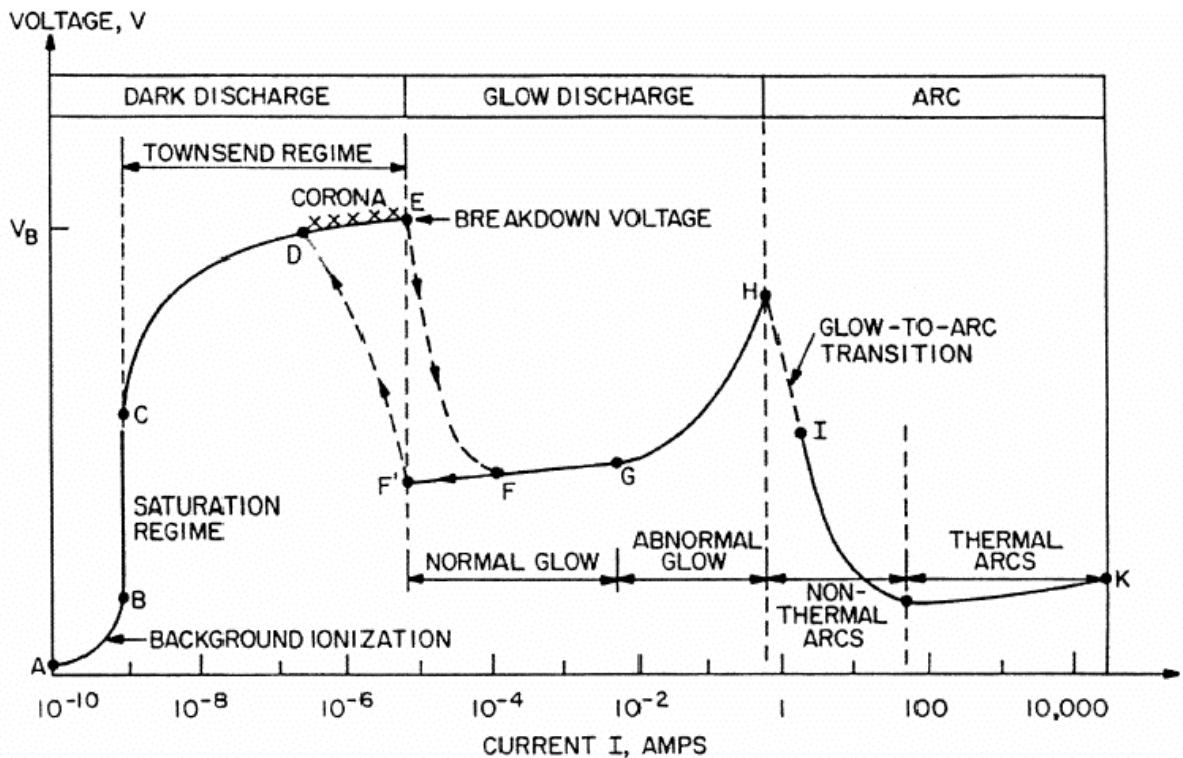


Figure 13 Spark behavior vs. current, from [Ref.19] Roth.



6.2 Model Results Comparisons

The model is run for the in-space and ground experiments presented in this paper. The best-fit results are compared in the tables below. Ground tests have similar operating regimes, likely due to the higher flow rate in ground equipment that uses a different mass flow delivery system than in-space.

Observations	Units	T11 In Space	T202405081004	T202405151412
Thrust	mN	37.49	29.64	37.04
Power (high voltage)	W	0.993	0.656	0.803
Mass Flow	ug/s	783	1,079	1,155

Preconditions	Units	T11 In Space	T202405081004	T202405151412
Water temperature	C	20	28	29
Vapor pressure	Pa	2,338	3,781	4,007
Voltage	V	967	875	1,018
Spark Paschen pd	Torr cm	5.03	0.77	0.83
n_{ie}	#/electron	38,844	901	1,574
Ion accel velocity	m/s	101,787	96,846	104,466
Electron accel velocity	m/s	18,440,706	17,545,532	18,925,995

Solution Quality	Units	T11 In Space	T202405081004	T202405151412
Sum(Abs(Error)/Meas)	ppm	0.0007	0.0138	0.0059
Constraints met?		Yes	Yes	Yes

Efficiencies	Units	T11 In Space	T202405081004	T202405151412
η_{beam}	%	55.3%	45.2%	47.4%
η_E	%	44.3%	54.4%	52.2%
η_{mass}	%	5.6%	5.3%	5.7%
Thrust:Power ratio	mN/W	37.8	45.2	46.1
I_{sp}	sec	4,880	2,802	3,271

Energy Usage	Units	T11 In Space	T202405081004	T202405151412
E_{cycle}	J/cycle	1.49E-03	9.84E-04	1.20E-03
$E_{cycle,ae}$	%	29.724%	23.490%	30.258%
$E_{cycle,ai}$	%	25.599%	21.708%	17.116%
$E_{cycle,g}$	%	44.277%	54.433%	52.228%
$E_{cycle,spark}$	%	0.000%	0.020%	0.011%
$E_{cycle,ir}$	%	0.400%	0.349%	0.386%
I_{spark}	A	6.06E-07	2.12E-05	1.42E-05



Thrust Sources	Column1	T11 In Space	T202405081004	T202405151412
ρ_{cycle}	Ns/cycle	5.62E-05	4.45E-05	5.56E-05
$\rho_{\text{cycle,ae}}$	%	0.000%	0.000%	0.000%
$\rho_{\text{cycle,ai}}$	%	0.013%	0.010%	0.007%
$\rho_{\text{cycle,g}}$	%	99.150%	98.508%	98.727%
$\rho_{\text{cycle,m}}$	%	0.000%	0.000%	0.000%
$\rho_{\text{cycle,cg}}$	%	0.837%	1.482%	1.266%
v_{ex}	m/s	11.82	12.23	11.46
dp	Pa	2,564	2,013	2,522
T_{dp}	C	21.49	28.00	29.00
$T_{\text{dp}}-T$	C	1.49	0.00	0.00

Mass Usage	Units	T11 In Space	T202405081004	T202405151412
m_{cycle}	ug/cycle	1.18	1.62	1.73
m_{hv}	%	5.592%	5.317%	5.724%
$m_{\text{hv,cg}}$	%	0.511%	0.786%	0.379%
m_{cg}	%	93.897%	93.897%	93.897%

Allocations	Units	T11 In Space	T202405081004	T202405151412
n_i	fraction	0.1453	0.0900	0.0918
n_{ae}	fraction	0.0089	0.0064	0.0073
n_{ai}	fraction	0.0077	0.0058	0.0042
n_{ri}	fraction	0.9911	0.9936	0.9927
n_{ti}	fraction	0.0012	0.0006	0.0032
$n_{\text{hv,cg}}$	fraction	0.0837	0.1288	0.0621



7. Water Propellant and Plasma Properties

Water’s vapor pressure is high enough to be useful in a passive feed system. Even when frozen, ice sublimates and has a useful vapor pressure. Further, water ion species include both high and low mass species, contributing to the imbalance that creates pressure-based thrust.

Water vapor pressure is given by the Arden Buck equation, originally presented in [Ref.1] and fully expanded in [Ref.2] and [Ref.3]. From [Ref.2], the Arden Buck equation for water vapor pressure is:

Equation 25

$$P = 611.21 e^{[(18.678 - \frac{T}{234.5})(\frac{T}{257.14 + T})]}$$

Where:

- P is the vapor pressure. Units: Pascal.
- T is temperature. Units: Celsius.

Temperature (Celsius)	Pascals	Torr	PSI
-10	286.6	2.15	0.04
0	611.2	4.58	0.09
10	1,227.9	9.21	0.18
20	2,338.3	17.54	0.34
30	4,245.1	31.84	0.62
40	7,382.4	55.37	1.07
50	12,349.4	92.63	1.79

Table 1 Water vapor pressure

In [Ref.4] III.B, Nakamura et al teach that the dominant ion species in water plasma are H₂O⁺, OH⁺, and H⁺ (i.e. proton). Others are possible but have significantly smaller ionization cross sections so are rare.

Nakamura et al model ionization of water vapor, including current and energy distribution by species. Two vapor injection locations, denoted “upstream” and “downstream” in the paper, are modelled. Of the two, “upstream” corresponds to the Poseidon™ injection method. Data is presented on the current density and numerical density of ion species in [Ref.4] Tables 1 and 2:

The averaged value of ion current density for each ion species at z = 4.0 mm.			
Species	H2O+	OH+	H+
j (A/m ²)	31.68	7.069	4.004

Table 2 [Ref.4] Table 1 water ion species current density, “upstream” location



The averaged ion number density of each ion species in the entire plasma region.			
Species	H2O+	OH+	H+
n (10 ¹⁴ /m ³)	265.7	57.83	8.088

Table 3 [Ref.4] Table 2 water ion species number density, “upstream” location

The net effect is that H⁺ ions (protons) are 9.4% of the current and 2.4% of the population count (in the reference’s relevant upstream region).

Using relationships between current (as number of ions/second) and local density, values are derived for average particle kinetic energy, kinetic energy density, and the fraction of kinetic energy ultimately allocated to each species.

Species	H2O+	OH+	H+
j (#/s/m ²)	1.9773E+20	4.4121E+19	2.4991E+19
v (m/s)	7,442	7,629	30,899
Kinetic Energy (eV/#)	5.17	5.13	4.98
KE density (J/m ³)	2.20E-02	4.75E-03	6.46E-04
KE fraction	80.3011%	17.3427%	2.3562%

Table 4 Water ion speciation energy relationships derived from [Ref.4]

Of key interest is that H⁺ ions have nearly the same kinetic energy as H₂O⁺ ions, albeit with a higher velocity due to reduced mass. Overall, the H⁺ ions gather 2.3562% of the kinetic energy imparted to all ions.

8. Proton-Boron Fusion

8.1 Background

At one point in the operating cycle, an ion sheath is present in the plume. The leading edge of this sheath is accelerated to high energy as it is both near to the electron sheath and repelled by the ions behind it. Of course, this acceleration acts to slow the lagging ions.

From Nakamura’s work [Ref.4], protons are present in the water ion products and obtain roughly the same kinetic energy as any ion species (all being singly charged). Being physically small, a proton has a large mean free path compared to other ions. Being low mass, a proton has a high velocity compared to other ions as well. These two properties essentially sort the ion sheath so that protons are the dominant species on the leading edge.

A proton of sufficient energy can induce nuclear fusion when colliding with a boron nucleus. There are multiple reaction pathways that depend upon energy level and the boron isotope. Of particular interest is the reaction of a proton with a boron-11 nucleus. This reaction is an initial fusion into a



highly unstable product that decays into 3 alpha particles, each about 2.9 MeV. Such a reaction is termed a “fusion evaporation” due to the immediate fission decay.

The reaction cross sections for protons with the two boron isotopes are shown below, with data taken from the EXFOR database. The alpha-producing reaction with boron-11 is the most probable at the lowest energy.

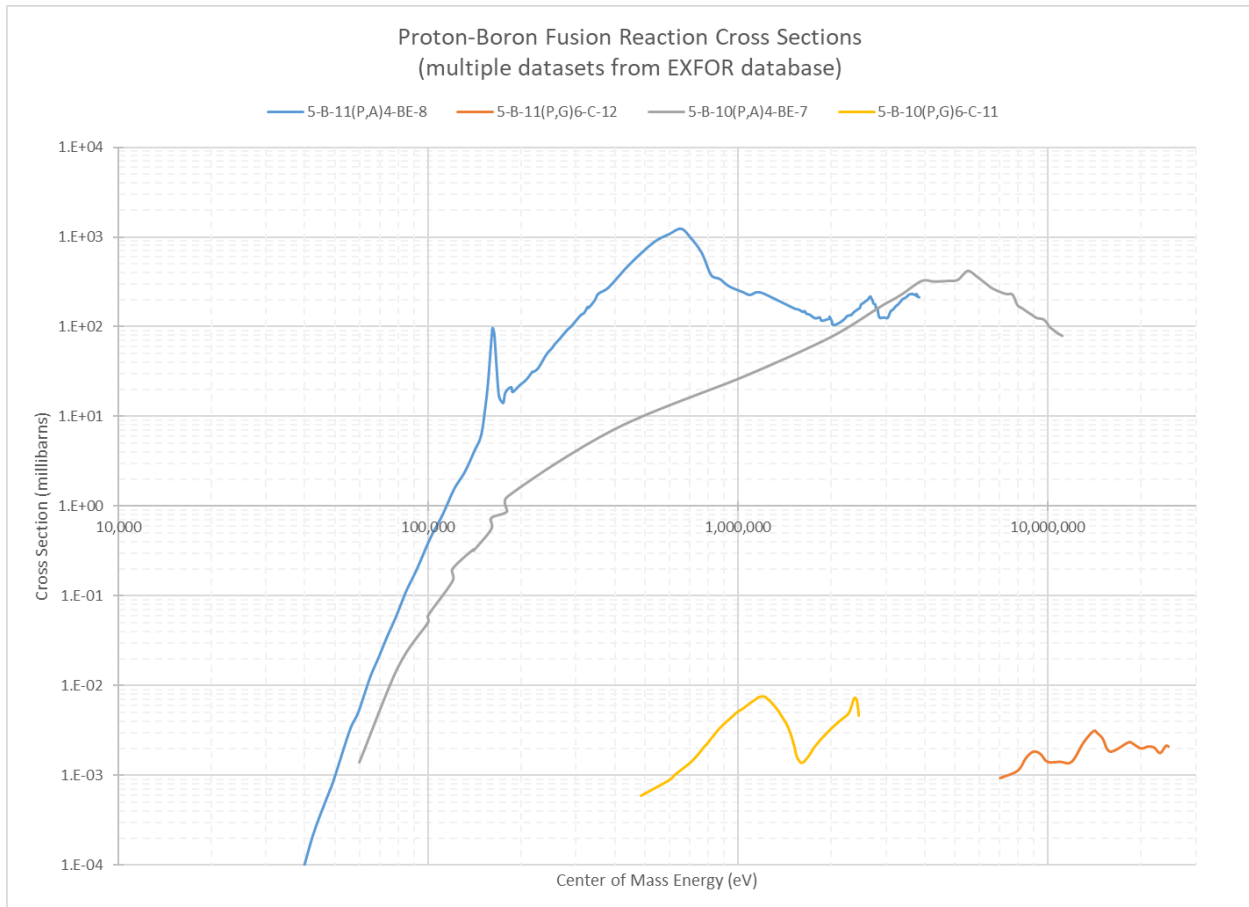


Figure 14 Proton-Boron fusion cross sections, wide view of energies

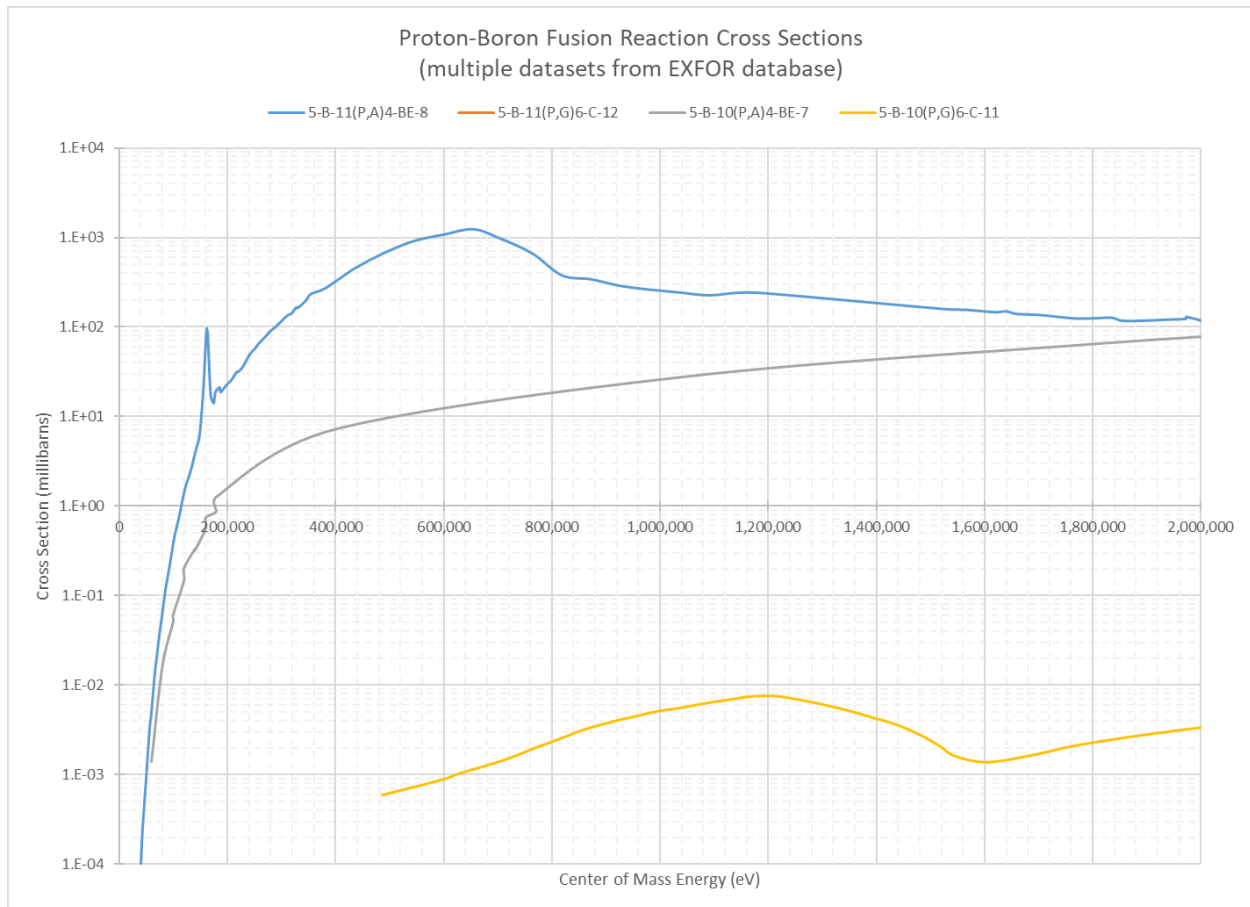


Figure 15 Proton-Boron fusion cross sections, detail view of energies

Simulations do predict plume protons reaching 600 keV. Being products of a wave leading edge, very few reach these energies. However few, some plume protons are expected to have enough energy to generate fusion with boron.

Of special note is the potential for gamma production at 600 keV energies. Boron has two natural isotopes. At this energy level, one isotope produces alpha particles, the other produces gamma rays (albeit with severely reduced probability). Physical tests for fusion use gamma rays as the telltale indicator of fusion given that sensors for alpha particles would physically interfere with the plume.

Production of alpha particles within the thruster plume has key benefits:

- Electron backflow is reduced due to ambipolar diffusion as the alpha particles induce the electron virtual cathode to flow outward. This expands the life of the plume ion sheath and should increase efficiency.
- Ion sheath density near the exhaust plane is increased from alpha particles flowing back toward the thruster. The increased density increases the pressure thrust from the trapped ions.



To achieve fusion benefits, boron-bearing vapor is injected into the plume region. This contrasts strongly with typical attempts at fusion within the reaction chamber interior where benefit is derived from heating reactants.

Thrusters were tested via simulation and physical experiments for their ability to generate pB fusion reactions within the exhaust plume. Physical tests were successful and lead to a granted US patent: US12129838B2 “Fusion Thruster” by Christopher Craddock and Wesley Faler.

8.2 Simulation of Proton-Boron Fusion

The Starfish simulator is used to simulate a 2D slice of the thruster. Starfish is an open-source project by Particle In Cell Computing (<https://www.particleincell.com/starfish/>). An open-source simulator was selected so that fusion reactions can be added as well as any proprietary electronics behaviors and enhanced reporting needed for validation of high energy reactions.

Starfish uses DSMC (Direct Simulation Monte Carlo) methods to accommodate the wide range of pressures, temperatures, and densities present in the thruster. The pressure range spans collision dominated regions/times to collisionless flows.

The simulator supports charge exchange reactions and impact ionization between electrons and neutral molecules. Simulations to date use the following species: H₂O, e⁻, H₂O⁺.

The simulator was updated to include proton-Boron fusion into alpha particles, recombination of electrons and ions into hot neutrals, and calculation of pressure-based thrust from first principles.

Simulation parameters that have been studied are: cycle timing, acceleration voltage, spark formation voltage, and gas temperature.

The spark is modeled as electrons being inserted into the volume near the negative spark electrode. Electron placement is random. Electrons are uniformly distributed throughout the entire spark duration.

Exhaust is directed in the +X direction. The simulator outputs momentum on each axis for each species at each timestep.

The simulation outputs the reaction momentum imparted to walls when a collision occurs. Conservation of Momentum is used to calculate the reaction momentum from particle/wall reflections.

Thrust is calculated as the average rate of change of accumulated +X momentum since the start of the spark (which occurs after initial conditions are established).

Energy balance is checked by ensuring the total energy present (kinetic, field, and potential) is less than the energy put into the system from the spark formation and initial field.

Fusion is simulated by introducing boronated water vapor into the exhaust plume. The boron source is water vapor containing 10,000 ug of boron per mL of liquid water. The flowrate of the carrier water vapor is set according to the experiment, maintaining the boron-to-water ratio.



Two configurations are studied, termed the “X” and “Y” configurations after their flow directions. The “X” configuration introduces vapor at the exhaust plane, flowing in the X-axis, expanding into the exhaust streams. The “Y” configuration introduces vapor at the exhaust plane as well, flowing upward to cross both streams. Like the pure water vapor used as propellant, the gas is at choked flow conditions, near the sonic speed limit.

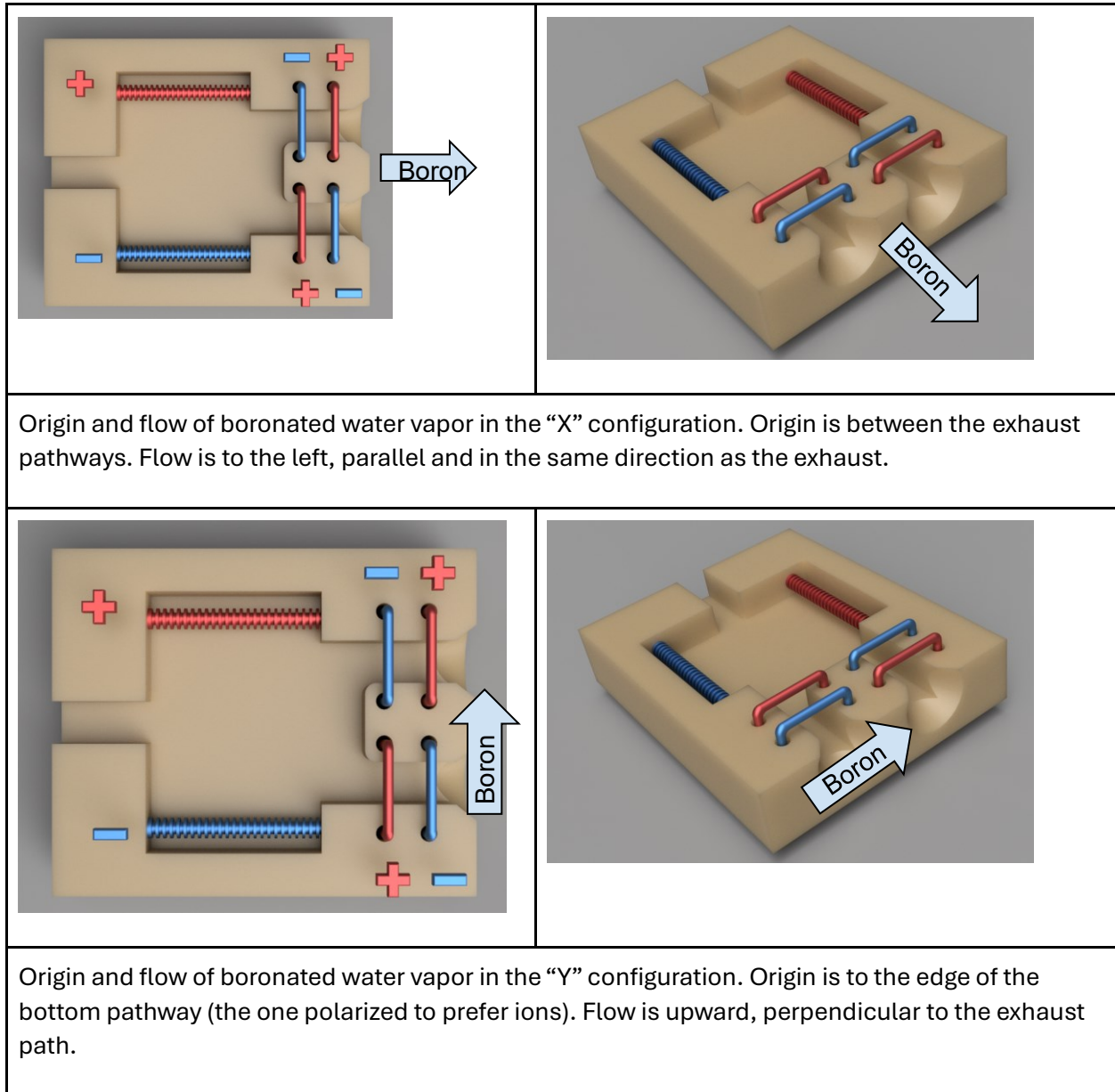


Figure 16 Boron vapor flow paths studied in simulation

In the “X” configuration, the boron plume expands vertically as it travels downstream. This gradually introduces the boron into the path of the ions. The rationale for the “X” configuration is to expand the boron into the highest speed ions which occur some distance downstream, causing low density boron to collide with high-speed ions.

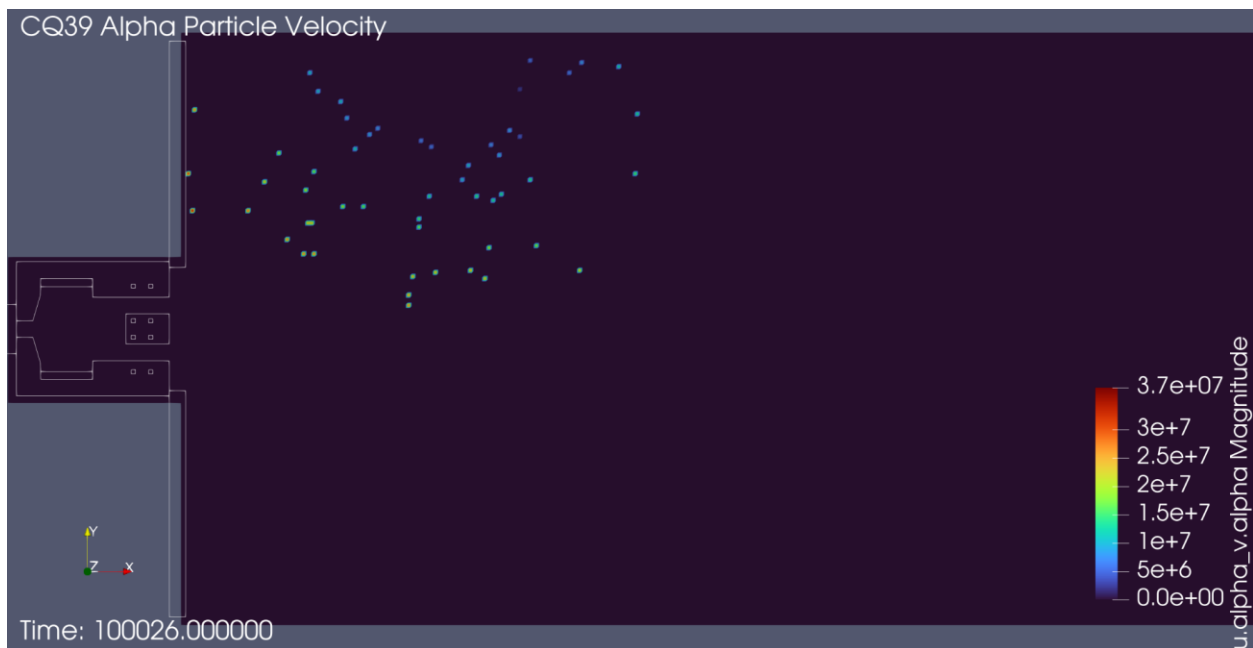


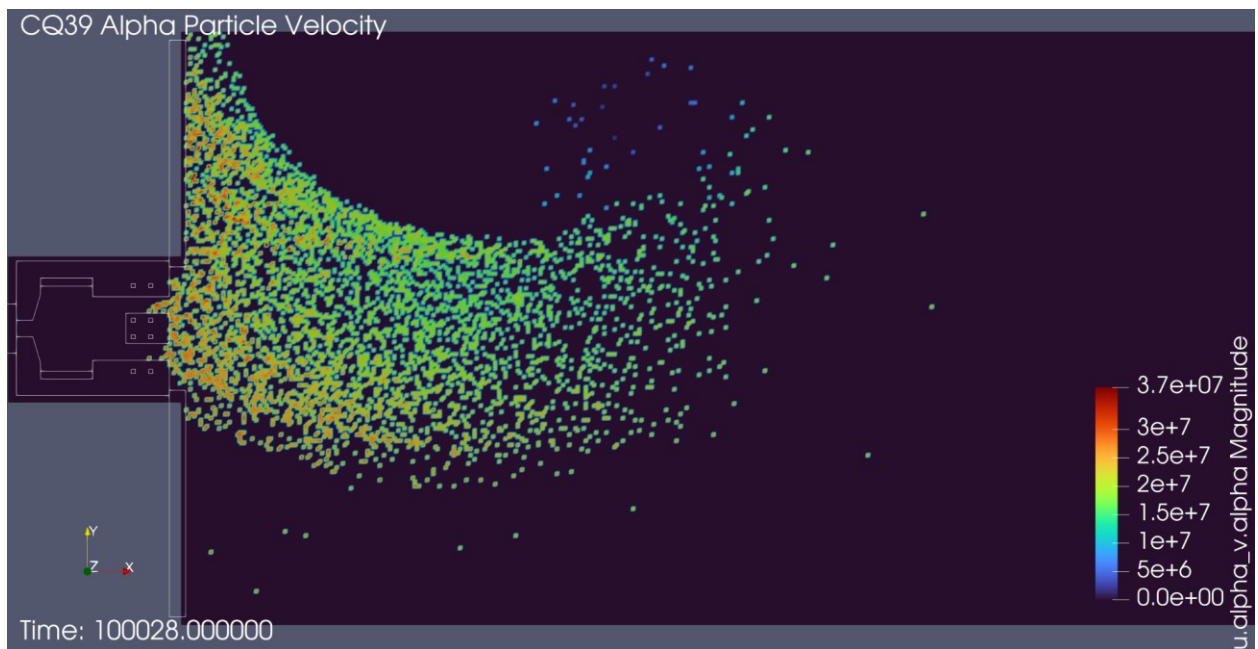
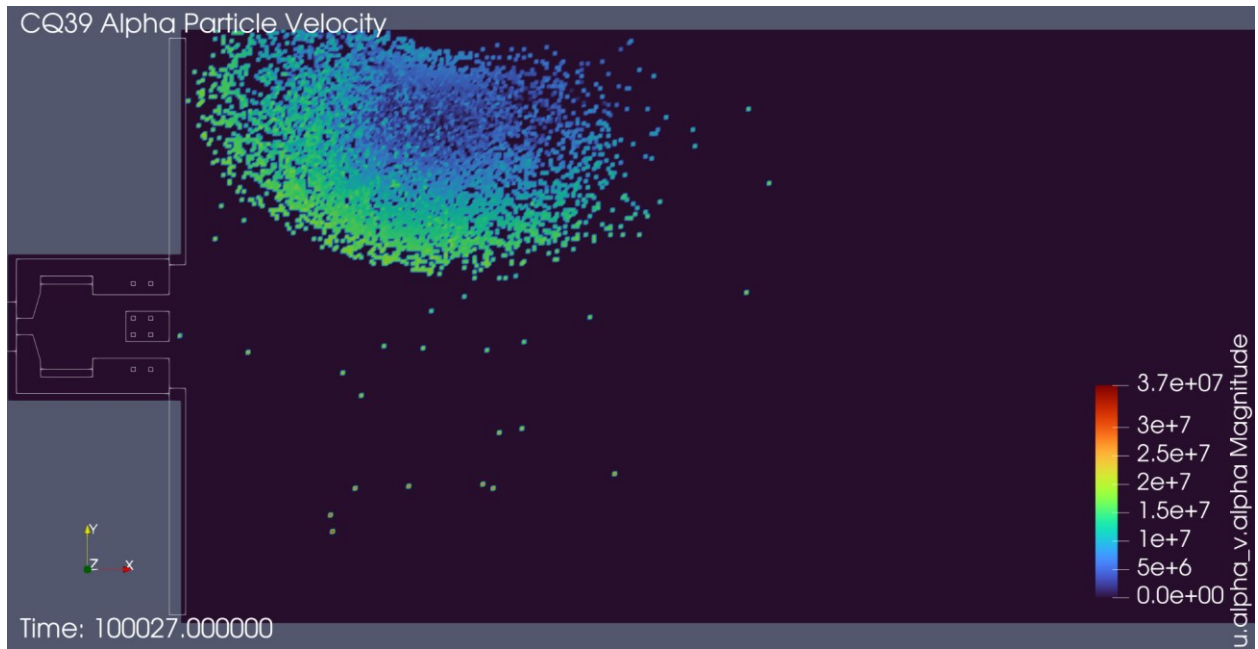
In the “Y” configuration, the boron plume expands horizontally as it travels upward. This forces low speed ions into high density boron regions. Given the low flow rates and vacuum conditions, boron migrates into the reaction chamber near the negative spark electrode.

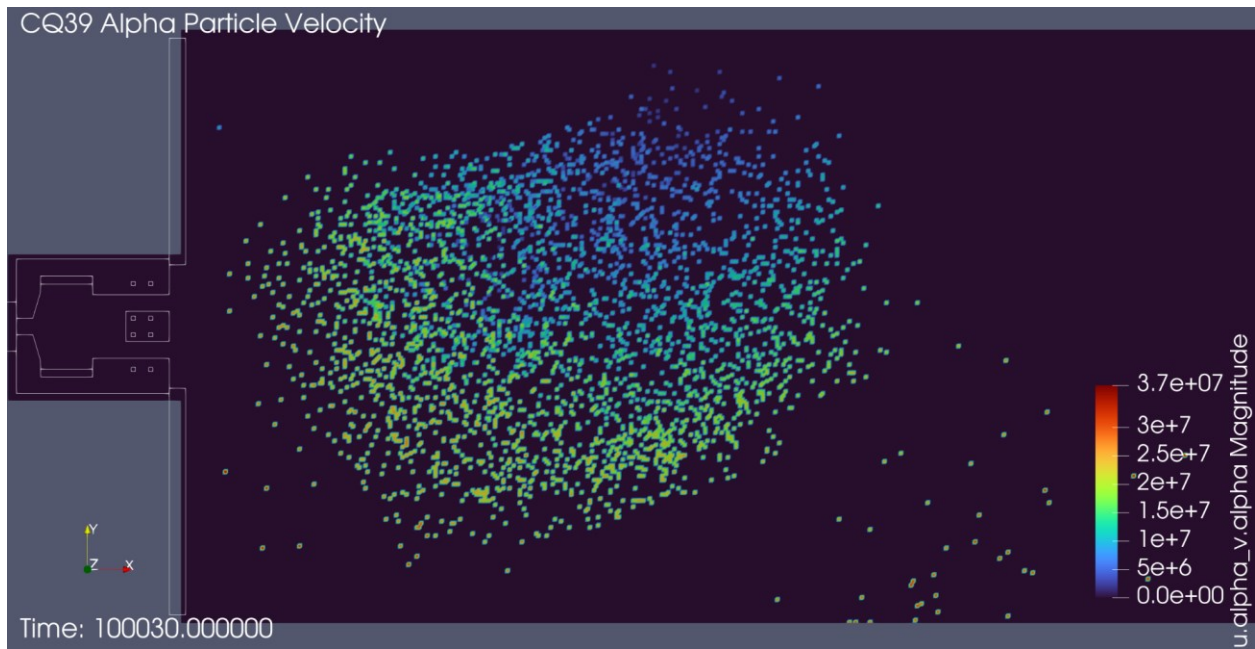
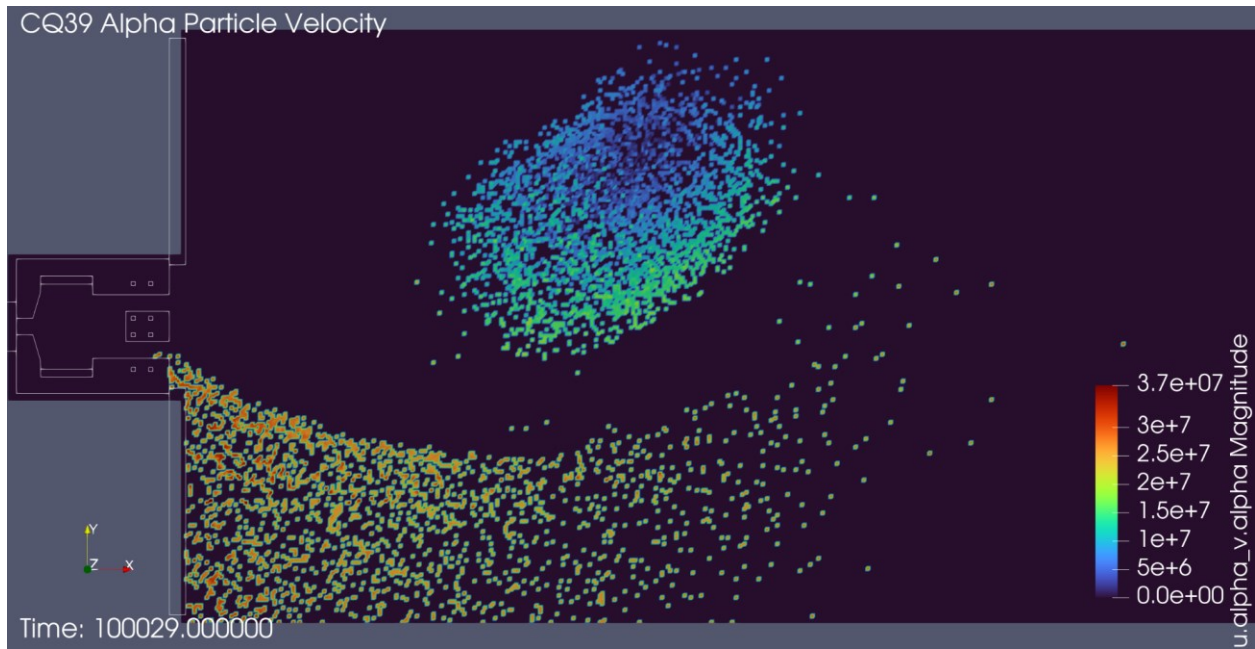
Fusion simulations are done using 100us (10,000Hz) cycles. This is in keeping with the conditions of previous physical experiments. The baseline case is 57ug/sec of water vapor propellant, an additional 57ug/sec of boronated water vapor, and operation at +/-500V.

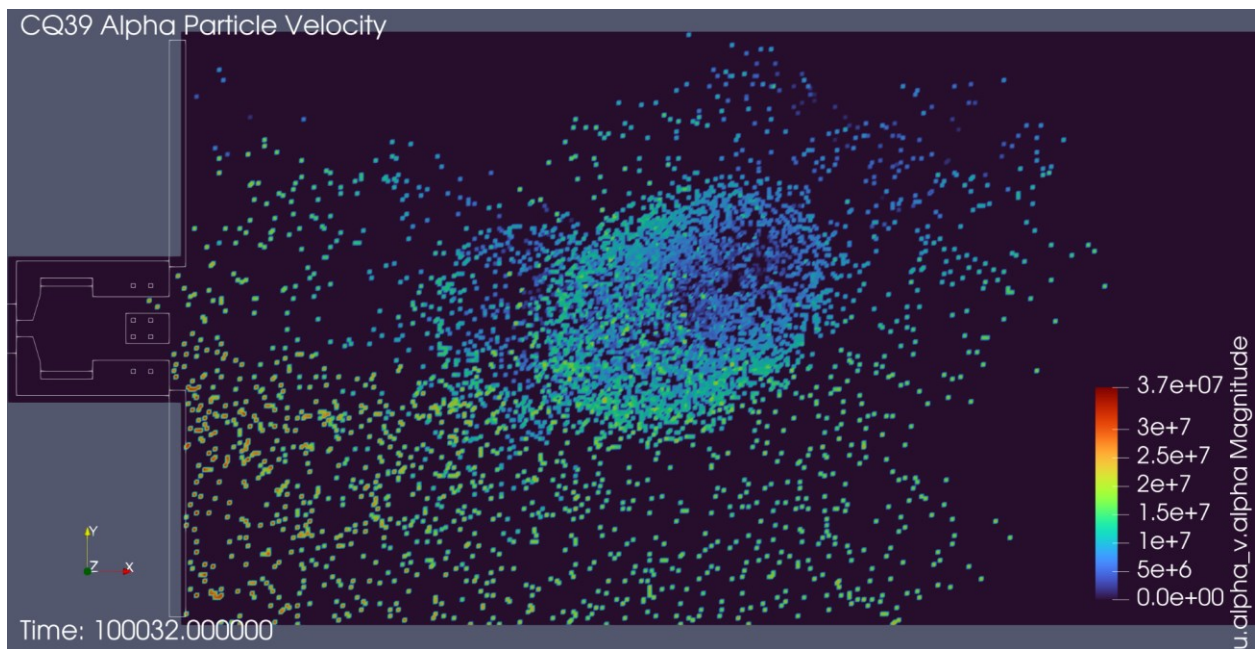
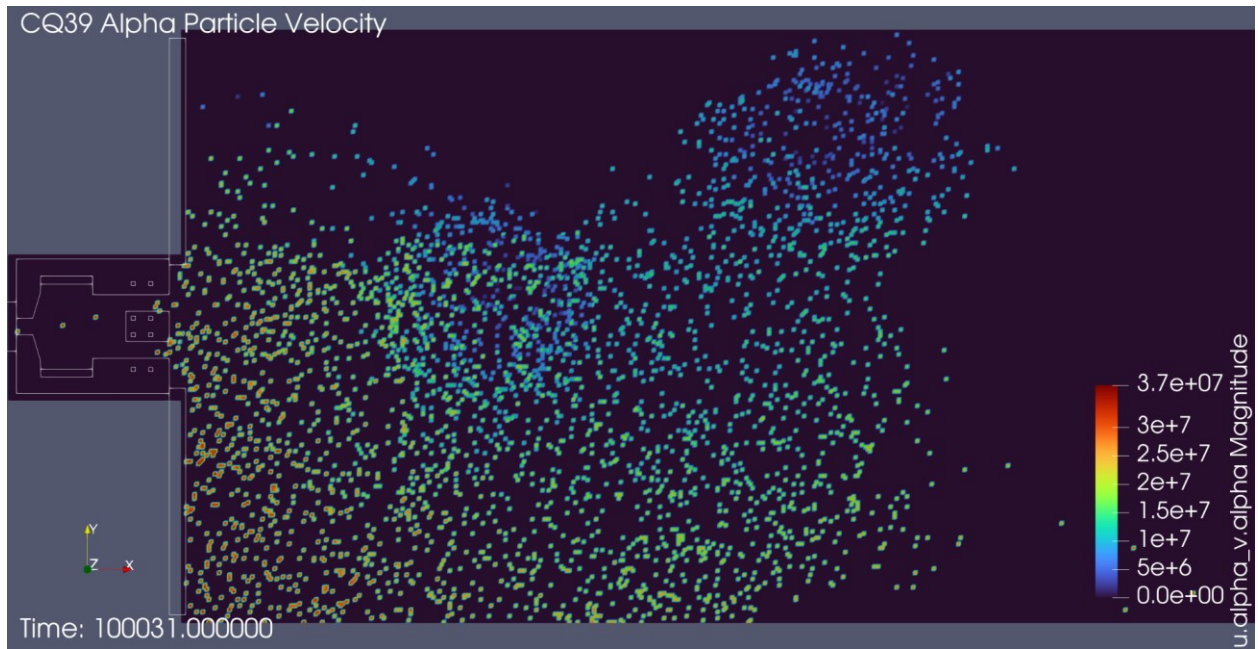
Fusion events from simulation CQ39 are shown below. In these, the thruster is at the left center. The dots are clusters of alpha particles, color coded by their absolute velocity. Alpha particle velocities up to about 35 million m/s are found (about 12% c). Direction is not depicted, though the alphas always spread out circularly from a region of fusion events. Not shown in these pictures is the effect of the alpha particles upon the plasma. The plasma effects can be deduced. Time index 100,026 shows sparse alphas from the first fusion region. The next timestep, 100,027, shows a large, dense alpha bubble. This can occur as ions are densified by the alpha wave disrupting the plume.

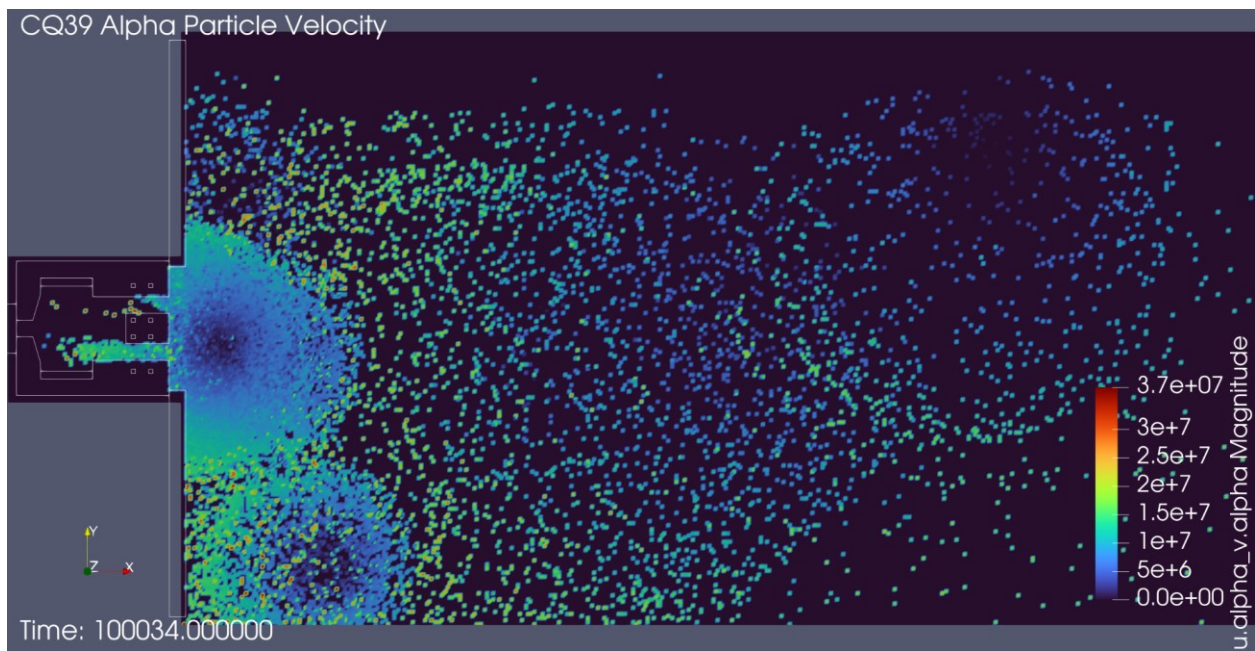
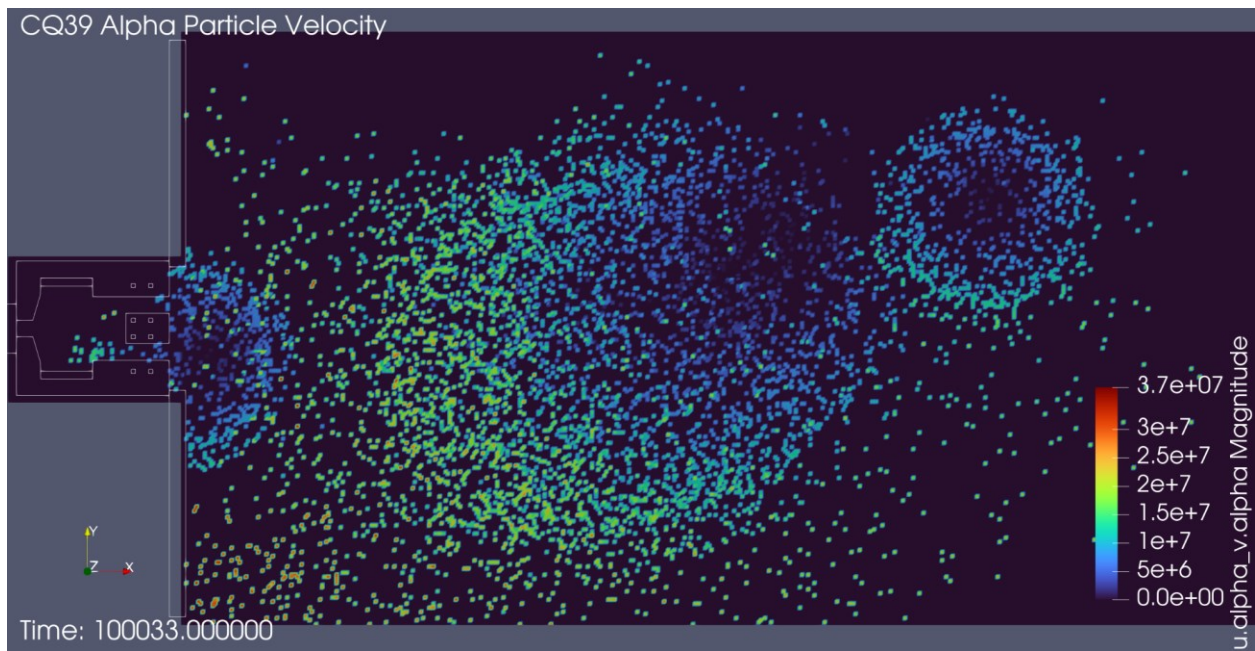
By time index 100,033, fusions are occurring within the immediate vicinity of the boron entrance, with some alpha particles migrating into the thrust head. Near that time, there are significant impacts of alpha particles upon the face plate. These impacts impart momentum. In simulation CQ47, those impacts alone give 4.26 mN of thrust - doubling the 4.2 mN thrust of the non-fusion thrust head.

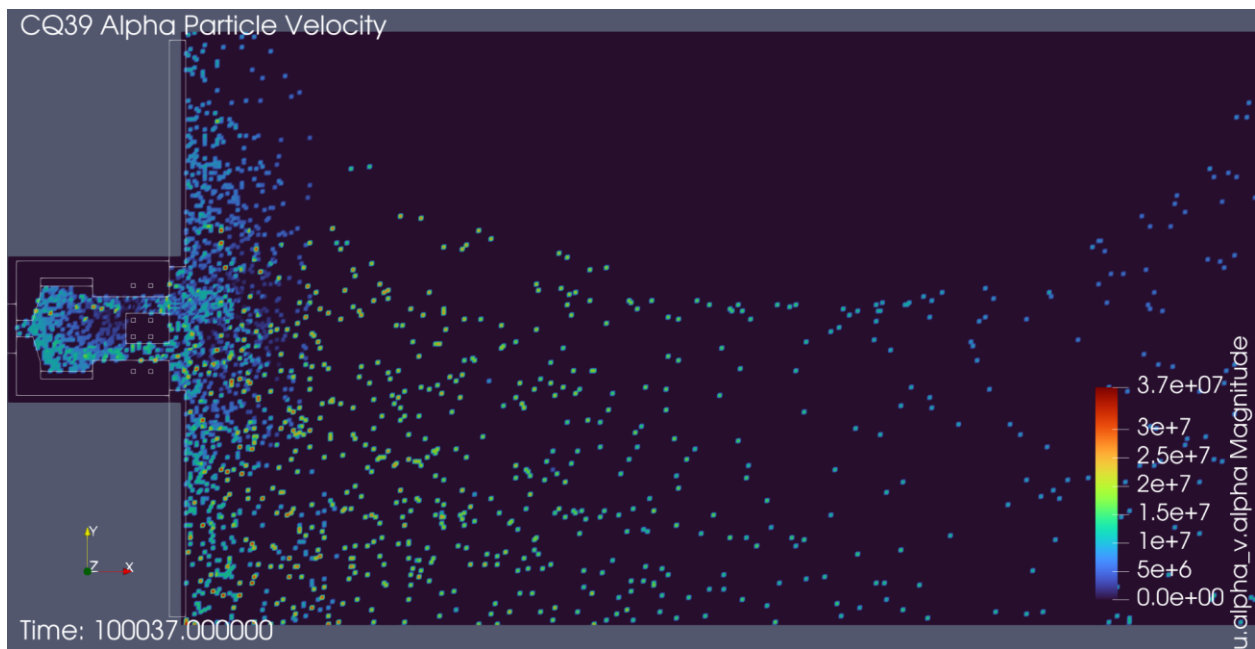
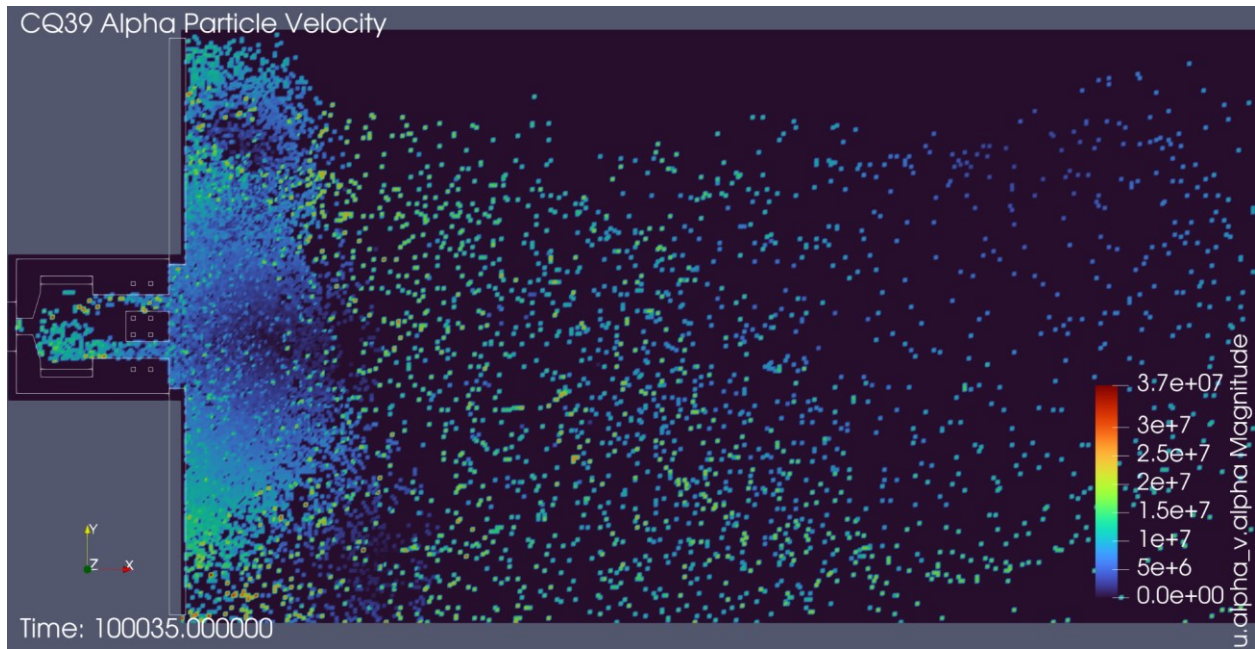














8.3 Physical Experiments

A single thrust head was placed within a vacuum chamber without a thrust stand. A solid-state gamma sensor was placed downstream of the device and monitored with an oscilloscope.

When running, a low light image shows the arrangement. Of note are the plume (two purple streams of different shapes - consistent with operational expectations), a center red light reflected from the camera itself, a green light in the lower right showing power present at the gamma sensor, and a yellow light in the lower corner showing a radiation detection event.

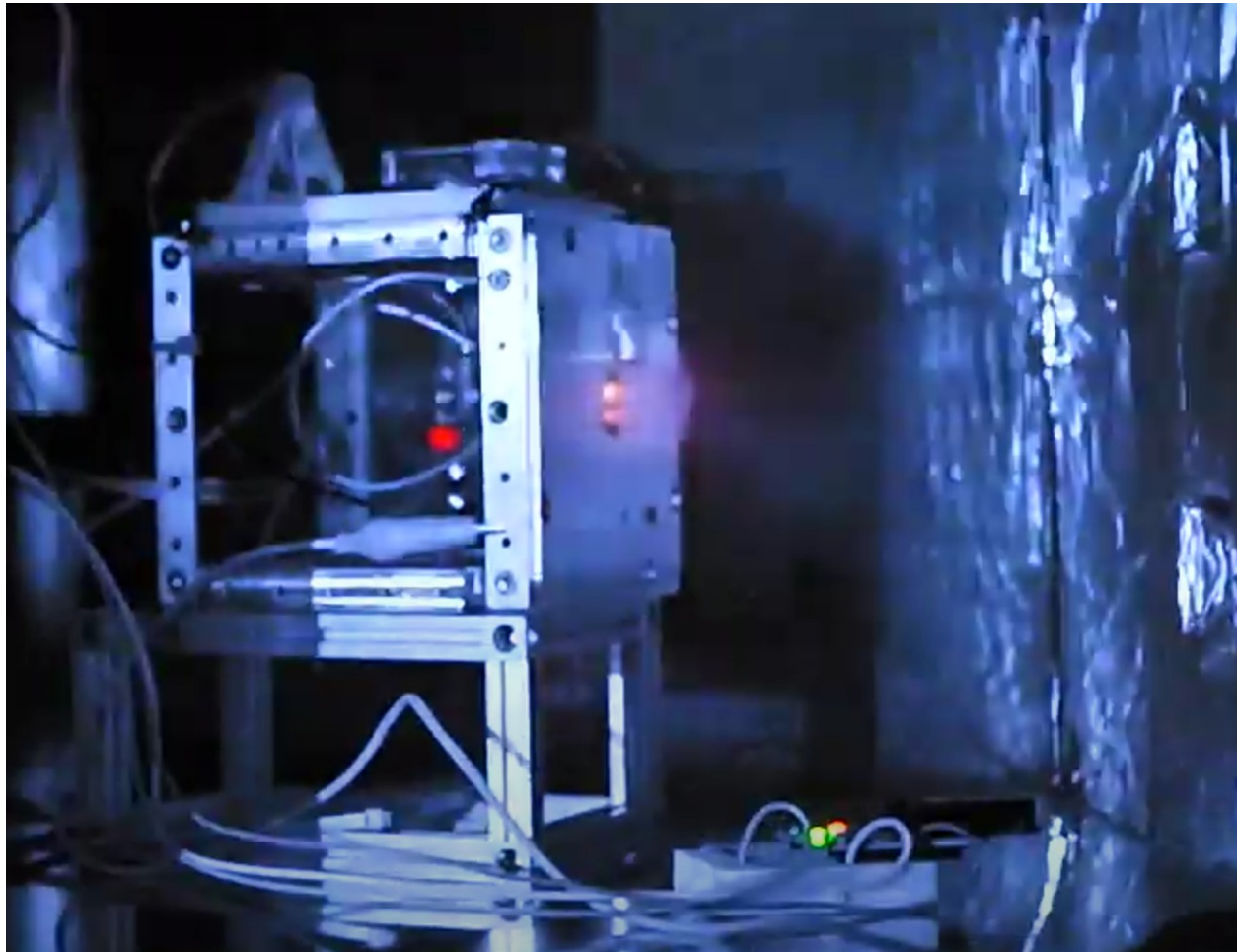


Figure 17 Single thruster operating with fusion events in the plume.

The gamma sensor is a BG51 sensor mounted with supporting electronics and sold as a MIKROE-4036 device. It triggers a 5V TTL pulse upon detection. Circuit inspection shows the pulse is a release of energy from a capacitor. When a second detection occurs before the first pulse has completed, the output waveform shows small spikes along the voltage decay rather than the ideal smooth signal decay. These secondary spikes are not counted by the oscilloscope.

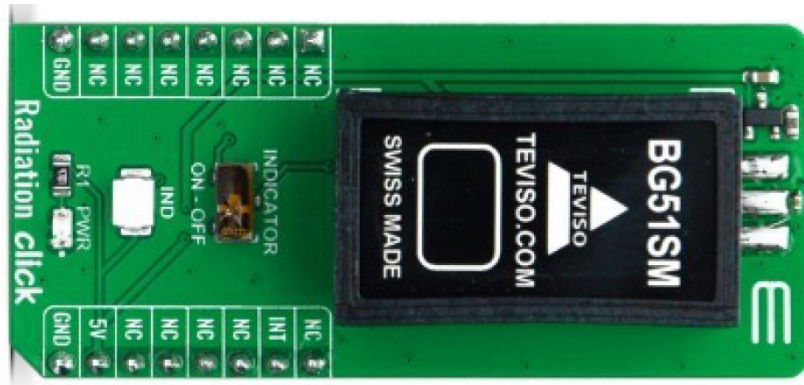


Figure 18 MIKROE-4036 sensor module

The radiation sensor is internal to the vacuum chamber. The center of its active window is approximately 9 cm downstream of the thruster face and 8.5 cm below the exhaust center line.

The thrust head is powered by two Emco high voltage supplies mounted externally to the vacuum chamber. One supply produces +500V when provided with 5V input. The other produces -500V at the same input. Output voltage is linearly proportional to input voltage with zero intercept and 1.5V minimum input needed for activation.

The two Emcos are powered by a benchtop power supply with variable voltage and current limiting features. The power supply readout shows voltage to 0.01V precision, amperage of 0.001A precision, and average DC power to 0.1W precision.

The digital output signal of the BG51 sensor is sensed using a digital storage oscilloscope. A single channel is used, resulting in a sampling rate of 1G Samples/second. The trigger is configured at 3.88V on the rising pulse edge. The trigger level was set experimentally to avoid line noise. The oscilloscope displays the rate of triggered events. When the rate is low, the rate is reported as “< 10Hz”.

A small radioactive sample is used to test the radiation sensor. The sample is a Geiger Counter Test Card from United Nuclear. It provides gamma and beta particles. The product information is at: https://unitednuclear.com/index.php?main_page=product_info&products_id=1005

The boronated water is a mixture of water and boron. It is made by SPEX CertiPrep, catalog number PLB9-3X. The mixture contains boron suspended in water in the concentration of 10,000 ug/mL. The boron used has a naturally occurring isotope ratio of 10B and 11B. As 10B fusion produces gamma rays, it is important that 10B is present in the boron supply.

When testing with the radioactive sample, pulses were present on the oscilloscope. An example pulse is shown below. It is approximately 210 us in duration at peak and another 500 us decay. The decay shape is typical of exponential decay curves of capacitive electronics. A pulse rate \leq 10Hz was reported by the oscilloscope.

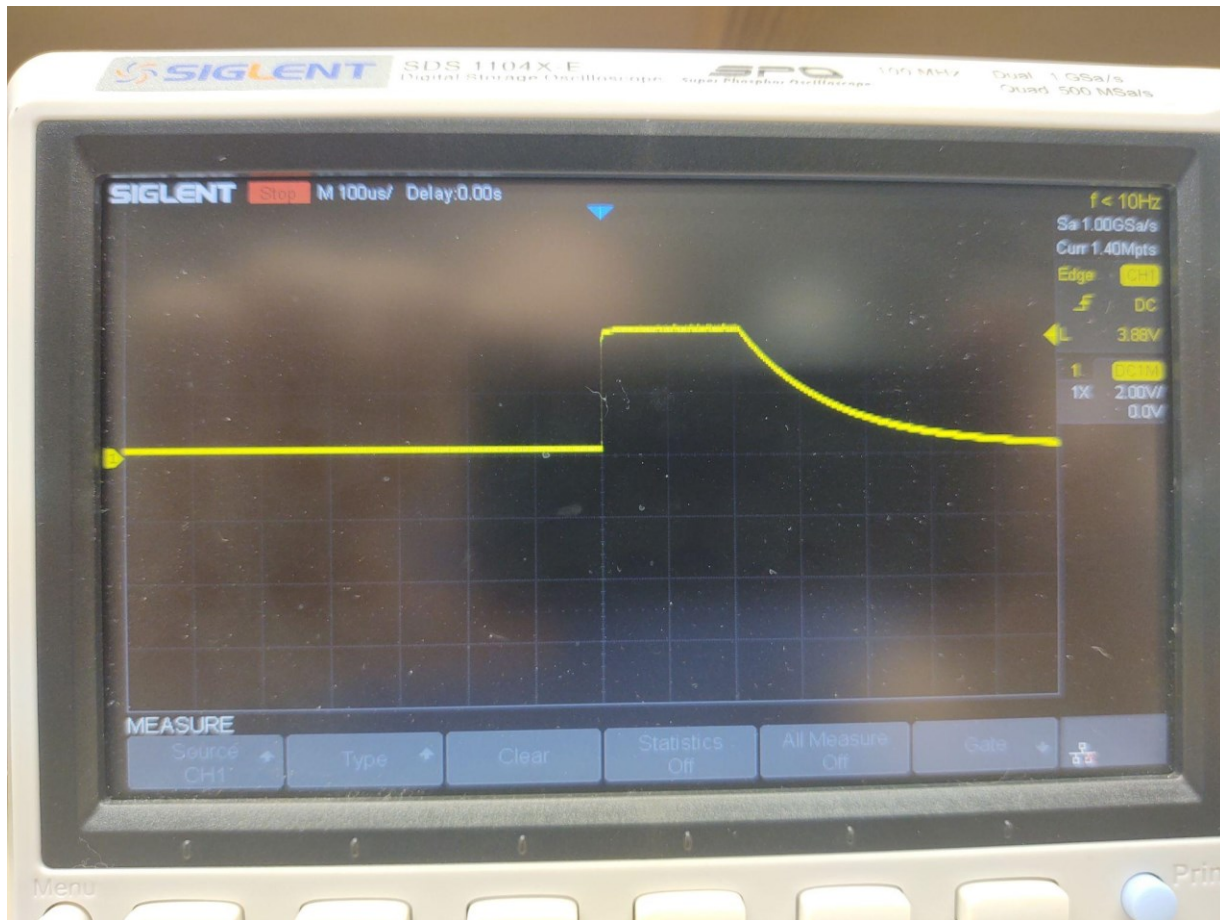


Figure 19 Gamma pulse signal from a radioactive sample

The thruster was first run as normal, using pure water propellant and pure water vapor injected into the plume. This establishes a baseline for false-positive detections due to other radiation sources in the plasma environment. Pulses were observed. A typical pulse is shown below. These arrived sporadically with a reported frequency of < 10Hz. Note the resemblance to the pulse with the radioactive sample.

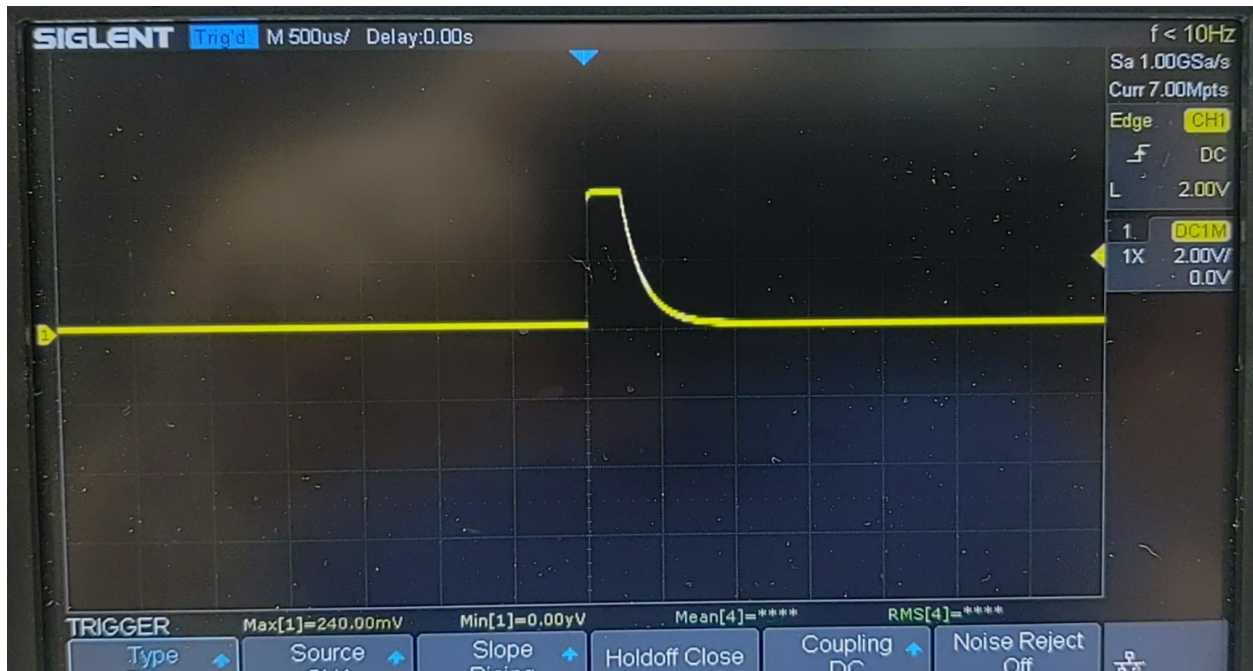


Figure 20 Signal pulse typical of running with pure water

While operating with boronated water at 4.5V low voltage input (+/- 450V acceleration voltage), radiation pulses were seen. The pulse rate was typically 400Hz and spanned 300-600Hz. Example pulses are shown below. Note the inclusion of secondary spikes unlike prior tests. These are expected from the sensor given a high incident rate. Manual counts of secondary peaks show 7-15 additional events per pulse.



Figure 21 Multiple gamma pulses using boronated water



Examples of single pulses follow:



Figure 22 Single gamma pulse using boronated water. Note secondary pulses during the decay period.

Changing the input voltage to 4.98V (and thus increasing the high voltage used for plasma acceleration to +/-500V), radiation detection events were registered at a higher frequency, typically 700+Hz, with a 500-800Hz range. Pulse shapes were the same as boronated water at 4.5V. An example pulse set is shown below. Manual counts showed similar secondary peaks of 7-15 additional events per pulse.



Figure 23 Multiple pulses using boronated water and higher acceleration voltage. Note increased frequency and strong secondary pulses.



8.4 Fusion Discussion

Experimental results show a clear and repeatable distinction between background radiation, baseline thruster operation, and active fusion conditions. When boronated water vapor is introduced into the exhaust plume, a significant increase in radiation detection is observed. This effect intensifies with increasing acceleration voltage, consistent with theoretical expectations for fusion activity.

The gamma detection events—recorded at frequencies ranging from hundreds to over 700 Hz—are notably absent during operation with pure water vapor. The shape and structure of the detected pulses show even higher event rates. These characteristics indicate multiple events within a short window and support the interpretation of genuine high-energy interactions that densify exhaust plasma as predicted in simulations.

The results align with simulation predictions showing that protons—originating from water vapor ionization and sorted to the leading edge of the ion sheath due to their high velocity and long mean free path—can achieve energies sufficient to induce proton–boron (p–B) fusion. The simulations suggest that even at modest acceleration voltages ($\pm 500\text{V}$), the dynamic structure of the ion sheath enables brief, localized conditions suitable for fusion. These conditions are not expected in conventional electric propulsion systems.

Importantly, fusion in this context is not pursued for energy gain or as a primary thrust mechanism. Instead, it serves as an experimental validation of the operating cycle. The presence of fusion-capable protons implies a structured and high-energy ion sheath, which in turn supports the theoretical basis for pressure-based thrust and the broader model of pulsed recombination-driven propulsion.

These findings mark a significant milestone: a fusion event occurring not in a reaction chamber, but within the exhaust plume of an electric thruster. This result, supported by both physical testing and simulation, reinforces the viability of the Poseidon™ thruster's operating theory and provides a novel lens through which future propulsion systems—especially those leveraging plume dynamics—may be designed and validated.

9. Conclusions

The Poseidon™ thruster represents a significant departure from traditional electric propulsion paradigms. By harnessing pressure-based thrust derived from controlled plasma recombination and pulsed operation, this system achieves high performance with minimal electrical input—delivering over 37 mN of thrust and specific impulse exceeding 4,800 seconds during in-space operation. These results, validated across multiple environments, affirm the viability of pressure-driven mechanisms in electric propulsion.

A full-system model grounded in mass, energy, and momentum conservation successfully predicts observed behavior, including thrust levels, power consumption, and mass flow characteristics. This



provides not only a theoretical framework but also a practical tool for future thruster design and optimization.

The observed occurrence of proton–boron fusion within the exhaust plume, supported by simulation and gamma detection, further validates the presence of high-energy protons and structured ion sheaths—key elements of the operating theory. While not a primary thrust source, fusion events substantiate the physical conditions predicted by the model and open doors to additional applications in space-based plasma systems.

Together, these results establish a compelling case for pressure-based thrust as a foundational design axis for next-generation electric propulsion. The Poseidon™ architecture demonstrates that high efficiency, high thrust-to-power ratios, and compatibility with water-based propellants are not mutually exclusive. This marks a step change in the capabilities available to small spacecraft, deep space missions, and rideshare platforms alike—offering new degrees of freedom in system design, mission planning, and resource utilization.

10. References and Additional Reading

1. Buck, Arden L. “New Equations for Computing Vapor Pressure and Enhancement Factor,” December 1, 1981. https://journals.ametsoc.org/view/journals/apme/20/12/1520-0450_1981_020_1527_nefcvp_2_0_co_2.xml.
2. “Vapor Pressure of Water Calculator.” Accessed October 22, 2024. <https://www.omnicalculator.com/chemistry/vapour-pressure-of-water#vapor-pressure-formulas>.
3. “Arden_Buck_Equation.” Accessed October 22, 2024. https://www.chemeurope.com/en/encyclopedia/Arden_Buck_Equation.html.
4. Nakamura, Kengo, Hiroyuki Koizumi, and Yoshinori Takao. “Investigation of Ion Species in Water Plasma Discharges for Miniature Microwave Discharge Ion Thrusters.” In *2018 Joint Propulsion Conference*. Cincinnati, Ohio: American Institute of Aeronautics and Astronautics, 2018. <https://doi.org/10.2514/6.2018-4650>.
5. Goebel, Dan M, and Ira Katz. “Fundamentals of Electric Propulsion: Ion and Hall Thrusters,” John Wiley & Sons, Ltd, 2008. Print ISBN:9780470429273, DOI:10.1002/9780470436448
6. “Mass Flow Choking.” Accessed October 23, 2024. <https://www.grc.nasa.gov/www/k-12/airplane/mflchk.html>.
7. NOAA / NESDIS / STAR website. “Center for Satellite Applications and Research - NOAA / NESDIS / STAR.” Accessed October 23, 2024. <https://www.star.nesdis.noaa.gov/star/index.php>.
8. Tsifakis, Dimitrios, Christine Charles, and Rod Boswell. “Comparison of Submillinewton Thrust Measurements Between a Laser Interferometer and a Load Cell on a Pendulum Balance.” *Frontiers in Space Technologies* 2 (April 27, 2021). <https://doi.org/10.3389/frspt.2021.632358>.
9. “Filtfilt — SciPy v1.14.1 Manual.” Accessed October 25, 2024. <https://docs.scipy.org/doc/scipy/reference/generated/scipy.signal.filtfilt.html>.



10. “Moving Average Filters: The Good and the Bad,” September 20, 2023.
https://www.makerluis.com/moving_average_filters/.
11. “State-of-the-Art of Small Spacecraft Technology - NASA.” Accessed October 28, 2024.
<https://www.nasa.gov/smallsat-institute/sst-soa/>.
12. Hsu, Andrea, and Andre Doumitt. “2023 Small Satellite Propulsion Technologies Compendium, The Aerospace Corporation, DISTRO A Version 1.4,” n.d.
13. Sutton, G.P., and O. Biblarz. Rocket Propulsion Elements, Ninth Edition. John Wiley & Sons (US), 2017.
14. Savage, Sam L, and Marc Van Allen. “THE FLAW OF AVERAGES IN LAW AND ACCOUNTING,” n.d.
15. Huser-Berta, Benjamin. “The Flaw of Averages — Comparing Monte Carlo Simulations with Estimates Based on Averages.” *Mastering Agility* (blog), December 22, 2023.
<https://medium.com/mastering-agility/the-flaw-of-averages-comparing-monte-carlo-simulations-with-estimates-based-on-averages-267528ae4f47>.
16. Sivoš, J., Škoro, N., Marić, D., Malović, G., & Petrović, Z. (2015). Breakdown and dc discharge in low-pressure water vapour. *Journal of Physics D: Applied Physics*, 48(42), 9
17. “Bernoulli’s Equation.” Accessed January 13, 2025.
https://www.princeton.edu/~asmits/Bicycle_web/Bernoulli.html.
18. Chung, Kyoung-Jae. “Electrical Breakdown in Gases,” 2018. Department of Nuclear Engineering of Seoul National University. "High-voltage Pulsed Power Engineering" course Fall 2018.
19. J Reece Roth, "Industrial Plasma Engineering [Volume 1: Principles]", The Institute of Physics, London, (2000)
20. Sutton, G.P., and O. Biblarz. Rocket Propulsion Elements, Ninth Edition. John Wiley & Sons (US), 2017.
21. Walter, Ulrich. *Astronautics*. Weinheim: Wiley-VCH, 2008.
22. Hill, P.G., and C.R. Peterson. *Mechanics and Thermodynamics of Propulsion*. Addison-Wesley, 1992.